Paleoceanography and Paleoclimatology

AGU ADVANCING EARTH AND SPACE SCIENCES

RESEARCH ARTICLE
10.1029/2022PA004578

Biomarker Records of Environmental Shifts on the Labrador Shelf During the Holocene

Henriette Kolling[1], Ralph Schneider[1], Felix Gross[1,2], Christian Hamann[3], Markus Kienast[4], Stephanie Kienast[4], Kristin Doering[4,5], Kirsten Fahl[6], and Ruediger Stein[6,7,8]

[1]Institute of Geosciences, Kiel University, Kiel, Germany, [2]Center for Ocean and Society, University of Kiel, Kiel, Germany, [3]Leibniz Laboratory for Radiometric Dating and Stable Isotope Research, Kiel University, Kiel, Germany, [4]Department of Oceanography, Dalhousie University, Halifax, NS, Canada, [5]Department of Geology, Lund University, Lund, Sweden, [6]Alfred Wegener Institute Helmholtz Centre for Polar and Marine Research, Bremerhaven, Germany, [7]Faculty of Geosciences, MARUM Center for Marine Environmental Sciences, University of Bremen, Bremen, Germany, [8]Key Laboratory of Marine Chemistry Theory and Technology, Ocean University of China, Qingdao, China

Abstract The ultimate demise of the Laurentide Ice Sheet (LIS) and the preceding and succeeding oceanographic changes along the western Labrador Sea offer insights critically important to improve climate predictions of expected future climate warming and further melting of the Greenland ice cap. However, while the final disappearance of the LIS during the Holocene is rather well constrained, the response of sea ice during the resulting meltwater events is not fully understood. Here, we present reconstructions of paleoceanographic changes over the past 9.3 Kyr BP on the northwestern Labrador Shelf, with a special focus on the interaction between the final meltwater event around 8.2 Kyr BP and sea ice and phytoplankton productivity (e.g., IP_{25}, HBI III (Z), brassicasterol, dinosterol, biogenic opal, total organic carbon). Our records indicate low sea-ice cover and high phytoplankton productivity on the Labrador Shelf prior to 8.9 Kyr BP, sea-ice formation was favored by decreased surface salinities due to the meltwater events from Lake Agassiz-Ojibway and the Hudson Bay Ice Saddle from 8.55 Kyr BP onwards. For the past ca. 7.5 Kyr BP sea ice is mainly transported to the study area by local ocean currents such as the inner Labrador and Baffin Current. Our findings provide new insights into the response of sea ice to increased meltwater discharge as well as shifts in atmospheric and oceanic circulation.

Key Points:

- Sea ice on the Labrador Shelf mainly follows the solar insolation and meltwater input from the decaying Laurentide Ice Sheet
- Sea ice increased following the Lake Agassiz outburst and Hudson Bay Ice Saddle Collapse between 8.5 and 8.2 Kyr BP
- Low sea ice conditions during the Holocene Thermal Maximum were replaced by an increase following the Neoglacial cooling trend

Supporting Information:

Supporting Information may be found in the online version of this article.

Correspondence to:

H. Kolling,
henriette.kolling@ifg.uni-kiel.de

Citation:

Kolling, H., Schneider, R., Gross, F., Hamann, C., Kienast, M., Kienast, S., et al. (2023). Biomarker records of environmental shifts on the Labrador Shelf during the Holocene. *Paleoceanography and Paleoclimatology*, *38*, e2022PA004578. https://doi.org/10.1029/2022PA004578

Received 7 NOV 2022
Accepted 21 AUG 2023

Author Contributions:

Conceptualization: Henriette Kolling, Ralph Schneider
Data curation: Henriette Kolling
Formal analysis: Henriette Kolling, Markus Kienast, Stephanie Kienast, Kristin Doering
Funding acquisition: Ralph Schneider
Investigation: Henriette Kolling, Felix Gross, Markus Kienast, Stephanie Kienast, Kristin Doering
Methodology: Henriette Kolling

1. Introduction

Recent climate warming is causing a decline of modern Greenland and Antarctic glaciers (e.g., Golledge et al., 2019). The resulting freshwater fluxes are key factors affecting the stability of the global heat distribution via ocean currents, and hence an improved understanding of their environmental consequences will critically enhance the quality of future climate predictions (e.g., Bakke et al., 2021; Rahmstorf, 1994; Stocker and Wright, 1991; Sundal et al., 2011; Williams et al., 2021). In addition to changes in sea level and the Earth's energy budget, the expected melting of continental glaciers will introduce large volumes of freshwater into the ocean. This freshening of the surface layer in polar and subpolar oceans will strongly affect ocean circulation and regional ecology. However, the response of sea ice and phytoplankton communities to large meltwater intrusions is not yet fully understood. The demise of the glaciers of the last glaciation may provide key insights into the natural mechanisms and consequences of such events.

Following the last glaciation, the ultimate demise of the Laurentide Ice Sheet (LIS) generated several meltwater pulses into the North Atlantic, of which the 8.2 Kyr event is the most studied example (e.g., Jennings et al., 2015; Klitgaard-Kristensen et al., 1998; Rasmussen et al., 2006, 2007; Rohling & Pälike, 2005; Stocker et al., 1992; Vinther et al., 2006). During this event, the drainage of the proglacial lakes Agassiz and Ojibway released ca. 163,000 km^3 of freshwater via Hudson Bay into the Labrador Sea and the North Atlantic (Barber et al., 1999; Jennings et al., 2015). The subsequent freshening of the subpolar gyre (SPG) is thought to have resulted in a reduced Atlantic Meridional Overturning Circulation (AMOC), leading to a nearly global atmospheric cooling (Barber et al., 1999; Ellison et al., 2006; Oster et al., 2017; Park et al., 2019; Thomas et al., 2007; Wiersma & Renssen, 2006; Yu et al., 2010). Most other smaller meltwater pulses are only recognized in local sedimentary records. For example, several sedimentary "red-beds" have been reported on the eastern Canadian Shelf between 9 and 7.5 Kyr BP, including an event around 8.6 Kyr BP (Jennings et al., 2015; Kerwin, 1996; Lajeunesse &

Validation: Felix Gross, Markus Kienast, Kristin Doering, Kirsten Fahl, Ruediger Stein
Visualization: Henriette Kolling
Writing – original draft: Henriette Kolling
Writing – review & editing: Henriette Kolling, Ralph Schneider, Felix Gross, Markus Kienast, Stephanie Kienast, Kristin Doering, Kirsten Fahl, Ruediger Stein

St-Onge, 2008). These events are characterized by negative stable oxygen isotope ($\delta^{18}O$) excursions and high detrital carbonate content that is related to ice rafting of Paleozoic carbonates previously eroded in the Hudson Bay area (MacLean, 2001). The event at ~8.2 Kyr BP is recognized by lighter stable oxygen isotope signatures of planktonic carbonate shells and a short-term cooling (Hoffman et al., 2012; Jennings et al., 2015; Lochte et al., 2019a; Thomas et al., 2007). However, some larger-scale studies suggest that a longer-term cooling trend already started around 8.65 Kyr BP or even 9 Kyr BP (e.g., Jennings et al., 2015; Rohling & Pälike, 2005) and other studies imply that much larger volumes of freshwater would have been necessary to cause the observed atmospheric cooling (Carlson et al., 2009; LeGrande & Schmidt, 2008; Meissner & Clark, 2006; Wiersma et al., 2006; Wiersma & Jongma, 2010). Lochte et al. (2019a) provide sedimentary evidence from the northwestern Labrador Shelf indicating that a smaller initial Lake Agassiz drainage event around 8.55 Kyr BP preceded the much larger Hudson Bay Ice Saddle collapse, which may have caused a significant freshening that led to the observed atmospheric cooling. After the final collapse of the Hudson Bay Ice Saddle, remnants of the large ice sheets remained in the Labrador, Keewatin and Foxe Ice Domes, which vanished almost completely by 5.8 Kyr BP (Dalton et al., 2020).

The Labrador Shelf provides an ideal location to study the ultimate demise of the LIS as it is located in the main outflow route of its final meltwater drainage (e.g., Jennings et al., 2015; Lochte et al., 2019a, 2019b; Rashid et al., 2014, 2019). Prior studies have focused on the oceanographic consequences of meltwater events caused by the final melting of the remaining ice sheets on the Canadian landmass. The link between abrupt freshwater events and sea ice has only been studied in the open northeastern Labrador Sea (You et al., 2023). The consequences of the final meltwater pulse around 8.2 Kyr BP from the LIS on sea ice over the Labrador Shelf, that is, within direct influence of the freshwater, is yet unknown.

A large number of proxies, including microfossil assemblages, provide indirect information about the presence/absence of sea ice (Cronin et al., 2013; de Vernal et al., 2001, 2013; Krawczyk et al., 2017; Seidenkrantz, 2013). However, the only proxy directly produced inside sea ice is a highly branched isoprenoid (HBI) with 25 carbon atoms, namely IP_{25} (Belt et al., 2007). IP_{25} is produced exclusively by specific diatom species inhabiting Arctic sea ice (Brown et al., 2014; Limoges et al., 2018) and appears to be a reliable and stable proxy for Arctic sea ice as far back as the Miocene (Belt, 2019; Belt et al., 2018; Stein et al., 2016; Stein & Fahl, 2013). The combination of the sea-ice biomarker IP_{25} with specific open-water phytoplankton biomarkers (i.e., brassicasterol, dinosterol and HBI III (Z)) in the so-called "PIP_{25}" index allows semi-quantitative estimates of sea-ice concentrations (Belt et al., 2015; Müller et al., 2011; Smik et al., 2016). However, the reliability of the different phytoplankton biomarkers used for the calculation of the PIP_{25} indices may differ between regions and result in different seasons represented in the resulting PIP_{25} indices (Kolling et al., 2020). Especially HBI III (Z), most likely produced exclusively in the marginal ice zone (Belt et al., 2015, 2019; Köseoğlu et al., 2018; Smik et al., 2016; Stein et al., 2017b), seems to yield more specific environmental information as it is produced by a smaller group of organisms compared to brassicasterol and dinosterol (Belt et al., 2015). Further, IP_{25} and HBI III (Z) have been found in similar concentrations in marine sediments, which simplifies the calculation of the PIP_{25} index (Belt et al., 2015; Smik et al., 2016).

Another frequently used biomarker is the sterol campesterol, which is produced by vascular land plants (e.g., Huang & Meinschein, 1979; Volkman, 1986; Yunker et al., 1995). In specific cases this sterol may also be produced by marine phytoplankton (Rontani et al., 2014; Volkman et al., 2008). However, this biomarker has been shown to reliably indicate terrigenous input into the Arctic Ocean, onto its shelf areas and in the Fram Strait (Fahl & Stein, 1997, 1999, 2007; Kremer et al., 2018; Xiao et al., 2013, 2015).

Here we present a record of the sea-ice proxy IP_{25}, along with other proxies for (open water) primary productivity and terrigenous input from a sediment core from the northwestern Labrador Shelf, covering the past 9.3 Kyr BP. We use these new data to explore (a) the response of sea ice during the increased meltwater discharge during the final demise of the LIS between 8.5 and 8.0 Kyr BP, and (b) the effects of varying meltwater influence on remaining sea-ice cover and primary productivity during the middle and late Holocene.

1.1. Regional Setting

The western part of the Labrador Sea is affected by the Labrador Current (LC), which flows southward along the shelf off Labrador and Newfoundland. The LC transports freshwater, sea ice, and icebergs to the subtropical

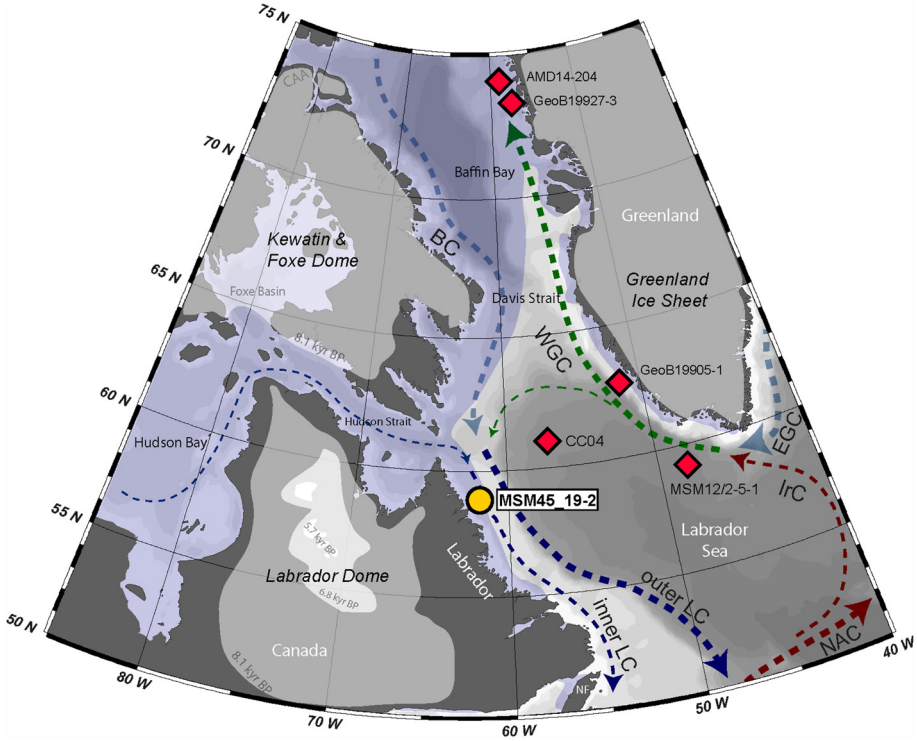

Figure 1. Modern surface circulation in the Labrador Sea and adjacent regions (adapted from Lochte et al., 2019b). The yellow dot indicates the location of sediment core MSM45_19-2 (this study). Red diamonds indicate other relevant core sites: CC04 (Gibb et al., 2015), GeoB199005-1 (Saini et al., 2022; Weiser et al., 2021), GeoB19927-3 (Saini et al., 2020), AMD14-204 (Limoges et al., 2020), MSM12-2-5-1 (You et al., 2023). The blue shaded area indicates the modern maximum sea-ice extent (spring; Cavalieri et al., 1996, updated 2017). The white shaded area indicates the extent of glaciers around 8.1 Kyr BP (Carlson et al., 2007; Dalton et al., 2020). Major surface currents are indicated in red (warm), blue (cold), and green (mixed). Abbreviations are as follows: BC, Baffin Current; EGC, East Greenland Current; IrC, Irminger Current; LC, Labrador Current; NAC, North Atlantic Current; WGC, West Greenland Current; NF, Newfoundland; CAA, Canadian Arctic Archipelago.

North Atlantic (Figure 1, Lazier & Wright, 1993) and is composed of two branches, the slower inner and the faster outer LC (Figure 1). The inner branch is mainly influenced by Davis and Hudson Strait outflow, with temperatures as low as −1.5°C and salinities below 34 (Lazier & Wright, 1993). It is approximately 100 km wide and reaches about 150 m water depth (Petrie & Anderson, 1983). Arctic freshwater from the Canadian Arctic Archipelago and riverine runoff via Hudson Strait is admixed to the inner LC (Figure 1). Changes in Hudson Strait outflow thus determine the water mass properties of the inner branch of the LC, which are ultimately transferred into the deep ocean (e.g., Dickson et al., 2008).

The outer LC branch transports the main volume of water (85%) and is mainly influenced by the West Greenland Current (WGC), composed of Atlantic Waters from the Irminger Current (Cuny et al., 2002; Myers et al., 2009), with temperatures around ~3.5°C and salinities around 35 (Lazier & Wright, 1993) as well as fresh, polar (0–1°C, salinities >30) waters from the East Greenland Current (EGC) (Aagaard & Coachman, 1968a, 1968b).

East of Newfoundland, close to the Flemish Cap and the Grand Banks, the LC encounters the North Atlantic Current (NAC), part of the northward flowing Gulf Stream (Fratantoni & McCartney, 2010). The mixing with the LC causes a freshening and cooling of the NAC, which result in increased density, sinking and the subsequent formation of the Labrador Sea Water (LSW) along the Labrador Slope (Czaja & Frankignoul, 2002), which forms the upper part of the North Atlantic Deep Water (Kieke & Yashayaev, 2015). During positive phases of the North Atlantic Oscillation (NAO), northwesterly winds carry cold Arctic air masses toward the Labrador Sea, the intense cooling of surface waters along the SPG that contains a significant proportion of saline Atlantic Water initiates enhanced deep convection and LSW formation (Clarke & Gascard, 1983; Pickart et al., 2002).

The sampling site on the Labrador shelf is located underneath the inner branch of the LC, close to Hudson Strait, and within the modern southern margin of Arctic sea-ice drift where sea ice is present for around 23 weeks

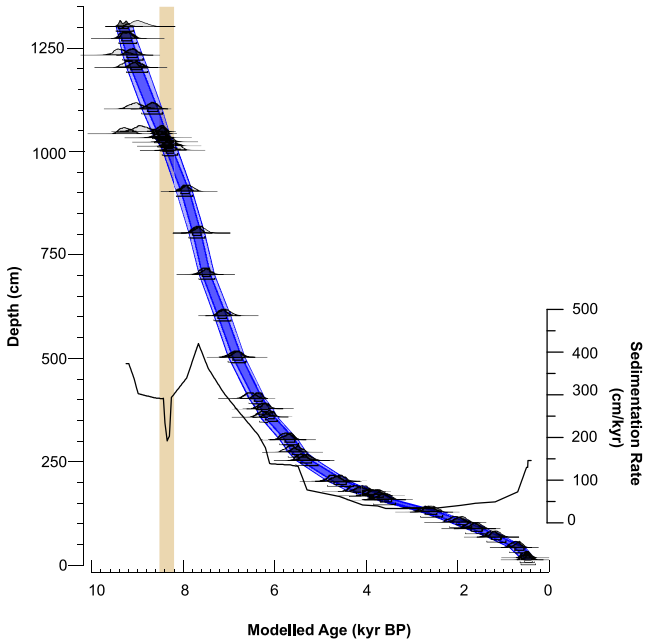

Figure 2. Bayesian age-depth model for sediment core MSM45_19-2 and sedimentation rates (cm/Kyr). The yellow bar indicates the freshwater peak based on benthic foraminifera (Lochte et al., 2019a).

annually (Figure 1; Cyr et al., 2021). Here, sea ice usually starts to form in December, extends southwards along the Labrador Shelf until the end of February and disappears in June/July (Cyr et al., 2021). Sea ice is not only formed locally but also advected from Hudson Bay and Davis Strait (Davidson, 1985).

2. Material and Methods

2.1. Materials

Gravity core MSM45_19-2 from the northwestern Labrador Shelf was obtained during R/V *Maria S. Merian* cruise MSM45 in 2015 (58°45.68′N, 61°56.25′W, water depth: 202 m) (Figure 1; Schneider et al., 2016). The homogenous olive gray, silty to clayey mud was sampled at 5 cm intervals on board. Samples were stored at 4°C on board and freeze-dried for further shore-based analytics.

2.2. Chronology

The new age model of Core MSM45_19-2 was constrained by 34 Accelerator Mass Spectrometry (AMS) radiocarbon dates of mixed benthic foraminifera (Table S1 in Supporting Information S1). Twenty-one of these AMS ages were presented previously by Lochte et al. (2019a, 2019b). We added 13 new age points in the upper 4 m of the core. To achieve best possible age estimates, a Bayesian Poisson-process deposition model, containing all available AMS ^{14}C ages of MSM45_19-2, was implemented in the software package OxCal v4.4.4 (Ramsey, 2008, 2009), using the marine data from Heaton et al. (2020) for calibration (Marine20) (Figure 2). The local marine reservoir offset was assumed to be 10 ± 80 ^{14}C years, based on the data of Coulthard et al. (2010) and McNeely et al. (2006). For the early Holocene, that is, before 7,000 cal BP, a sea-ice correction of 200 ± 50 ^{14}C years was added for a total offset of 210 ± 90 ^{14}C years (Lewis et al., 2012). As the varying influx of radiocarbon depleted freshwater from Lake Agassiz-Ojibway prior to the Hudson Bay Ice Saddle collapse is influencing the radiocarbon dates (Lochte et al., 2019a), we implemented an outlier model, allowing the according radiocarbon determinations to be shifted by up to 1,500 years toward older ages. For sample KIA-52591 ($z = 1{,}303$ cm) no freshwater offset was implemented in the final model, because otherwise only a poor agreement between its radiocarbon determination and modeled age was achieved. The sample at 3 cm, closest to the surface, had to be excluded from the final age model, because the radiocarbon content is too high to allow calibration using the marine data set. The high radiocarbon content is likely indicative of bomb ^{14}C from after 1950 originating from reworked sediments from the missing sediment surface of the sediment core, lost during the coring process. For details see Table S1 in Supporting Information S1.

2.3. Biogenic Opal Determination

Biogenic opal (BSi) was determined at Dalhousie University via wet-alkaline digestion following the method of Mortlock and Froelich (1989). About 20 mg of the freeze-dried samples were treated with 2 mL of 10% H_2O and 10% HCl, followed by sonication to remove carbonate and organics and to disaggregate the sediment. Afterward, sediment samples were dissolved in 2M $NaCO_3$ in a 85°C water bath for 5 hr, and repeatedly swirled about once per hour. The amount of dissolved silica was determined by molybdate-blue spectrometry. Long-term precision ($n = 16$, over 2 years, 1SD) of in-house standards was ±1.2% for a JV_A (12.3% opal) and ±0.45% for MESS_3a (3.2% opal). Duplicate measurements of samples, available for a third of the samples, resulted in precision (1SD) between 0.1% and 1.9%

2.4. Biomarker Analyses

The total organic carbon (TOC) content was determined using an ELTRA, CS-800 Elemental Analyzer on freeze-dried and homogenized sediment samples after the removal of carbonates with hydrochloric acid

(37%, 500 µL). The concentrations of specific biomarkers were analyzed on 4–5 g of freeze-dried sediments. Samples were extracted by sonication (3 × 15 min) using dichloromethane:methanol (2:1 v/v; 30 mL). Prior to biomarker extraction two internal standards, 7-HND (7-hexylnonadecane, 20 µL/sample) and androstanol (5α-androstan-3β-ol, 20 µL/sample), were added for quantification purposes. Hydrocarbon and sterol fractions were separated by open-column chromatography with SiO_2 as stationary phase. For hydrocarbons, *n*-hexane (5 mL) and for sterols, ethylacetate:*n*-hexane (2:8 v/v; 7 mL) were used as eluent. Sterol fractions were silylated using 200 µL BSTFA (2 hr, 60°C).

Hydrocarbon concentrations were determined using an Agilent Technologies 7890 gas chromatograph (30 m HP-1MS column, 0.25 mm in diameter and 0.25 µm film thickness) coupled to an Agilent Technologies 5977 A mass selective detector. Sterol concentrations were measured with an Agilent Technologies 6850 GC (30 m HP-1MS column, 0.25 mm in diameter and 0.25 µm film thickness) coupled to an Agilent Technologies 5975 A mass selective detector. All compounds were identified by comparing their retention times to those of reference compounds (IP_{25}: Belt et al., 2007; HBI II: Johns et al., 1999; HBI III: Belt et al., 2000; sterols: Boon et al., 1979; Volkman, 1986). IP_{25} and HBI III (Z) (IP_{25}: m/z 350; HBI III (Z): m/z 346) were quantified by the abundant fragment ion m/z 266 of the internal standard 7-HND. Sterols were quantified as trimethylsilyl ethers (brassicasterol: m/z 470, campesterol: m/z 472, dinosterol: m/z 500) in regard to the molecular ion of androstanol (ion m/z 348). The different responses of all these ions were balanced by external calibration. For details see Fahl and Stein (2012). During each analytical sequence, instrument stability was controlled by reruns of external standards and replicate analyses of random samples.

All biomarker concentrations were normalized to both the extracted weight of sediment (µg/gSed) and TOC (µg/gTOC). Accumulation rates (µg/cm^2/year) were calculated using the following equations (e.g., Stein & Macdonal, 2004):

$$\mathrm{MAR} = \mathrm{SR} \times \mathrm{DBD} \quad (1)$$

$$\mathrm{TOC\ AR} = \mathrm{MAR} \times \mathrm{TOC}/100 \quad (2)$$

$$\mathrm{BM\ AR} = \mathrm{MAR} \times \mathrm{BM} \quad (3)$$

with MAR = Mass Accumulation Rate (g/cm^2/year), SR = sedimentation rate (cm/year), DBD = dry bulk density of each sample (g/cm^3), TOC = total organic carbon (weight percent), BM = biomarker concentration (µg/gSed), AR = accumulation rate. Equation 2 was also applied to calculate BSi accumulation rates.

After the determination of biomarker concentrations, the PIP_{25} indices were calculated as follows:

$$PIP_{25} = [IP_{25}]/([IP_{25}] + ([PM] \times c)) \quad (4)$$

with PM representing the specific phytoplankton marker, that is, brassicasterol (P_BIP_{25}), dinosterol (P_DIP_{25}) or HBI III (Z) ($P_{III}IP_{25}$). The balance factor *c* is the ratio of mean IP_{25} concentration and mean sterol concentration, counterbalancing the generally higher concentrations of sterols compared to IP_{25}. HBI III (Z) and IP_{25} showed similar concentrations in the initial studies from the Barents Sea, which led to the assumption that the balance factor *c* is unnecessary in the calculation of the $P_{III}IP_{25}$ index (Belt et al., 2015; Smik et al., 2016). However, findings from northern Hemisphere surface sediments indicate that this may not be the case everywhere (Kolling et al., 2020). The applicability of the PIP_{25} indices on the northern Labrador Shelf will be discussed in the Discussion, Section 4.2.

3. Results

Sedimentation rates vary greatly in sediment core MSM45_19-2 (Figure 3), documenting a major change in the sedimentation regime around 6.2 Kyr. Prior to 6.2 Kyr BP, the Labrador Shelf was strongly influenced by glacier runoff and sediment plumes and sedimentation rates as high as ca. 450 cm/Kyr. Around 6.5 Kyr BP, when the largest remnants of the Labrador Dome melted during its termination after the last glaciation (Dalton et al., 2020), the sedimentation rates decreased drastically (<100 cm/Kyr) and became hemipelagic with low to moderate terrestrial input (Lochte et al., 2019a, 2019b). The lowest sedimentation rates (<100 cm/Kyr) are observed during the last 5 Kyr BP. This shift has to be accounted for when interpreting sedimentary concentrations of different proxies in core MSM45_19-2. For example, concentrations and accumulation rates of TOC and

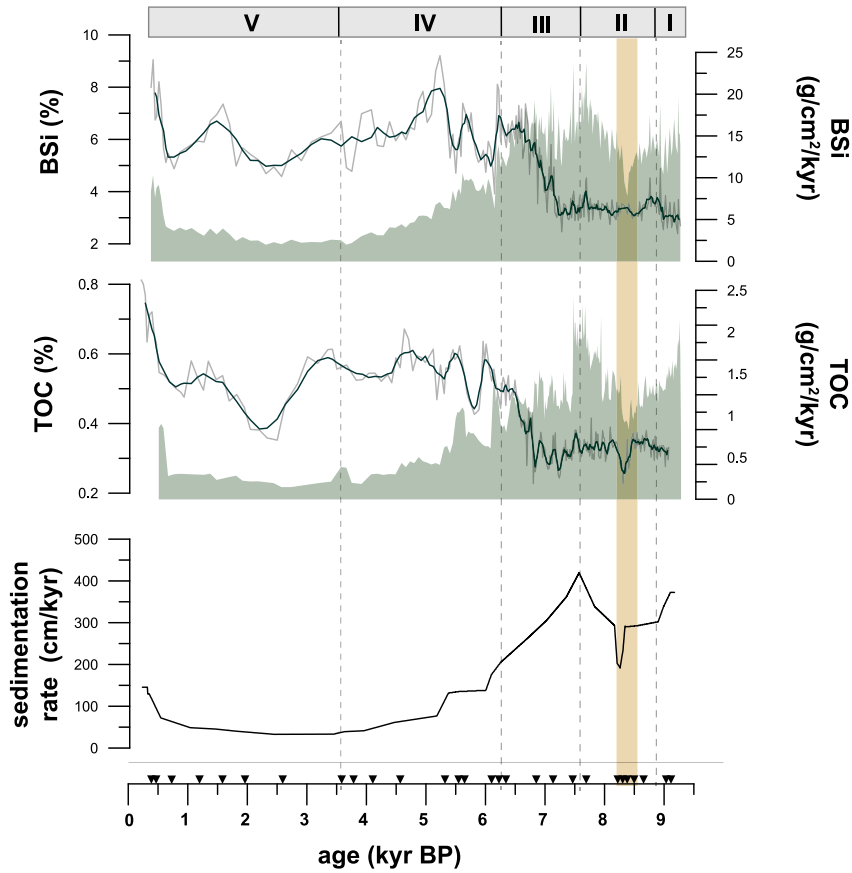

Figure 3. Bulk parameters of Core MSM45_19-2. Concentrations of biogenic opal (BSi; in %; gray line: concentration, green line: 5pt running average) and its accumulation rate (in g/cm^2/Kyr; green area), total organic carbon (TOC) concentration (in %; gray line: concentration, green line: 5pt running average) and its accumulation rate (in g/cm^2/Kyr; green area) and sedimentation rate in (cm/Kyr). The vertical yellow bar indicates the period of maximum meltwater outflow based on stable oxygen isotopes ($\delta^{18}O$) of benthic foraminifera (Lochte et al., 2019a). The roman letters indicate the different intervals referred to in Section 4. Discussion. Black triangles indicate radiocarbon dates.

BSi (Figure 3) show contrasting trends with concentrations lowest prior to 6.8 Kyr BP whereas accumulation rates are highest in this oldest core section (Figure 3). We will describe and interpret both concentrations and accumulation rates of the sedimentary components here, to prevent over interpretation of signals that may be caused by shifts in sedimentation rate rather than environmental changes.

Biomarker concentrations are presented in µg/gTOC here. Concentrations in µg/gSed show the same trends (Figure S1 in Supporting Information S1).

TOC and BSi concentrations show the lowest values, around 0.3% and 3% respectively, from 9.3 to 6.8 Kyr BP. After that, they rise to higher values (~0.55% and 6%) and show synchronous oscillations for the remainder of the record (Figure 3). Concentrations of the sea-ice biomarker IP_{25} are lowest from 9.3 to 8.9 Kyr BP (~0.1–0.2 µg/gTOC) and rise gradually toward a peak around 8.2 Kyr BP (~0.8 µg/gTOC) (Figure 4). This peak is followed by decreasing concentrations which reach intermediate values around 7.5 Kyr BP (~0.4 µg/gTOC). IP_{25} concentrations then remain constant until 4 Kyr BP, rising continuously thereafter toward highest values in the modern samples (~1.6 µg/gTOC) (Figure 4). The marginal ice zone biomarker HBI III (Z) is present in very low concentrations (~0.1 µg/gTOC) until 8.5 Kyr BP when concentration rise to a prominent peak, reaching the highest values between 8.2 and 7.5 Kyr BP (~9 µg/gTOC) (Figure 4). HBI III (Z) concentrations drop toward low (~0.4 µg/gTOC) values which begin to increase from ~3.7 Kyr BP toward the core top (~1 µg/gTOC) (Figure 4). The phytoplankton biomarkers brassicasterol and dinosterol show lowest concentrations between 9.3 and 8.9 Kyr BP (~3 µg/gTOC and ~8.8 µg/gTOC, respectively) (Figure 4). Both start to increase around 8.9 (~12 µg/gTOC and ~13.5 µg/gTOC), but while dinosterol concentrations remain relatively high until 6.4 Kyr BP, brassicasterol concentrations decrease around 8.2 Kyr BP (Figure 4). Afterward, both proxies are present in low/intermediate

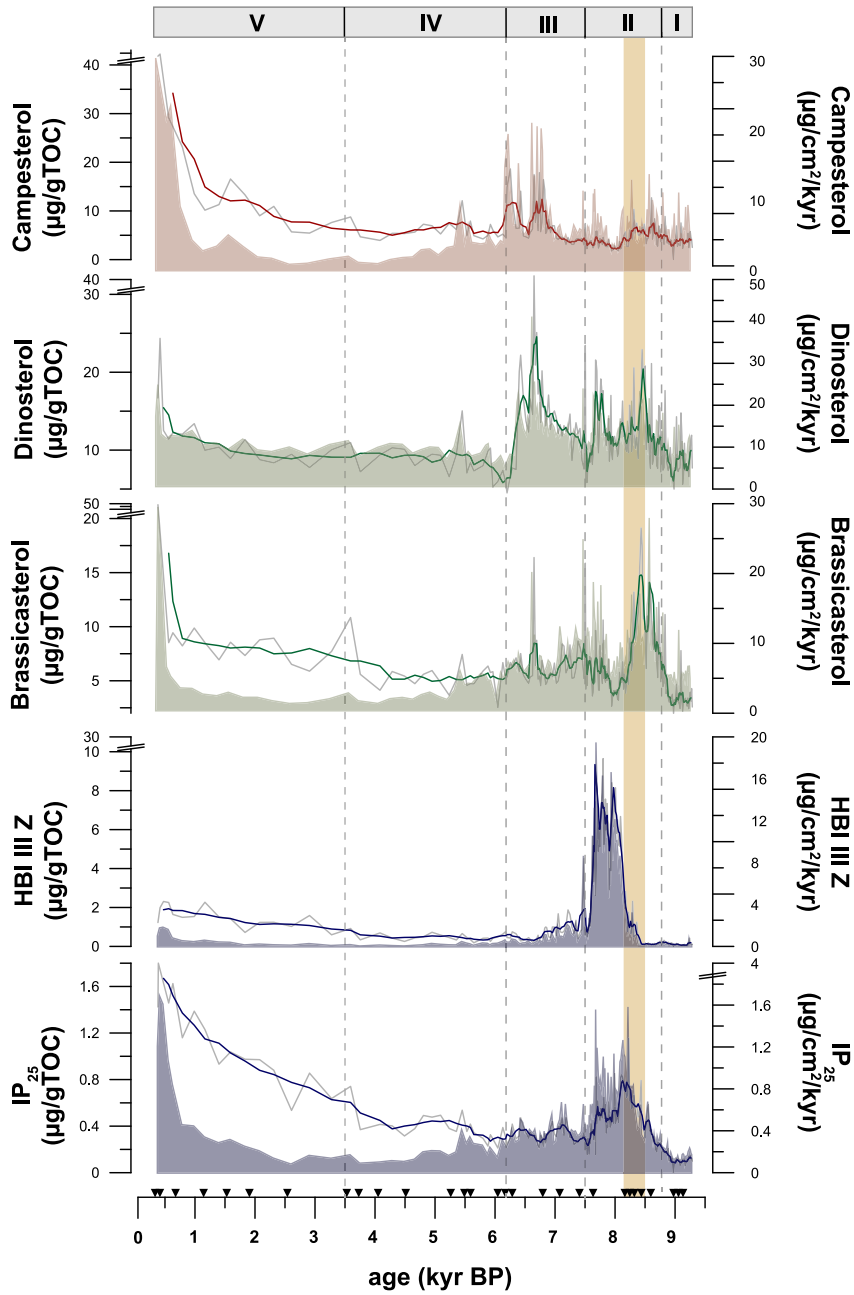

Figure 4. 5-pt running average of concentrations (line, in µg/gTOC) and accumulation rates (area, in µg/cm^2/Kyr) for specific biomarkers of core MSM45_19-2. Campesterol (red), dinosterol (green), brassicasterol (green), HBI III (Z) (blue) and IP_{25} (blue) against age before present (Kyr BP). The vertical yellow bar indicates the period of maximum meltwater outflow based on stable benthic oxygen isotopes $\delta^{18}O$ (Lochte et al., 2019a) shown in Figure 7. Black triangles indicate radiocarbon dates.

concentrations, which start to gradually rise again around 3.7 Kyr BP toward the core top (Figure 4). Campesterol concentrations, associated with terrigenous input, show low concentrations between 9.3 and 7.1 Kyr BP (~5 µg/gTOC) (Figure 4). Between 7.1 and 5.5 Kyr BP intermediate concentrations (~10 µg/gTOC), with several peaks, are observed. Afterward, campesterol concentrations start to rise to their highest values at the core top (~36 µg/gTOC) (Figure 4).

Accumulation rates of TOC and BSi follow the sedimentation rate (Figure 3), with highest values between 9.3 and 6.1 Kyr BP (~1.4 and ~15 g/cm^2/Kyr). These high values are interrupted by a reduction in accumulation

rates between ~8.5 and 8.2 Kyr BP (1 and 10 g/cm^2/Kyr) paralleled by a short-lived reduction in sedimentation rates during the same period (Figure 3). However, concentrations of TOC in particular show a similar decreasing trend, indicating less influence of the sedimentation rate on the accumulation rate. For both proxies, accumulation rates decrease continuously toward 3.8 Kyr BP. For the last 3.8 Kyr BP accumulation rates increase again slightly (Figure 3).

For the biomarker records, accumulation rates follow the trend of concentrations (Figure 4). IP_{25} accumulation rates show low values between 9.3 and 8.9 Kyr BP (0.2 μg/cm^2/Kyr), high values between 8.2 and 7.2 Kyr BP (1 μg/cm^2/Kyr) (Figure 4). After 7.5 Kyr BP, IP_{25} accumulation is low (0. 1 μg/cm^2/Kyr) (Figure 4). For the last 4 Kyr BP, IP_{25} shows increasing accumulation rates toward the core top (5 μg/cm^2/Kyr) (Figure 4). HBI III (Z) is absent in most of the record, except for a strong peak in accumulation rates between 8.5 and 7.5 Kyr BP (15 μg/cm^2/Kyr) and slightly elevated values from 7.5 to 7.0 Kyr BP (1 μg/cm^2/Kyr) (Figure 3). Accumulation rates of brassicasterol and dinosterol all show similar trends, with intermediate accumulation rates for the interval from 9.3 to 8.9 and 6.4 Kyr BP, respectively (5 and 10 μg/cm^2/Kyr), followed by a gradual decrease toward the lowest values between 5.5 and 2 Kyr BP (2.5, 10 μg/cm^2/Kyr). In the youngest core section, the last 1 Kyr BP, accumulation rates rise to high values (brassicasterol: 30 μg/cm^2/Kyr, dinosterol: 35 μg/cm^2/Kyr) (Figure 4). Accumulation rates of campesterol are intermediate in the lowest core section (5 μg/cm^2/Kyr), and show three higher peaks around 7, 6.4, and 5.6 Kyr BP (Figure 4). Campesterol accumulation is low between 5.5 and 2 Kyr BP (0.0025 μg/cm^2/year) and rises to the highest accumulation rates toward the core top (30 μg/cm^2/Kyr) (Figure 4).

4. Discussion

As illustrated in previous studies by Lochte et al. (2019a, 2019b), sediment core MSM45_19-2 presents an ideal archive for the Holocene postglacial paleoceanographic changes on the northwestern Labrador Shelf. The new high-resolution proxy records presented here, provide additional and detailed information about changes in sea-ice conditions, terrigenous input and marine primary productivity.

4.1. Sources of Productivity Proxies

Previous studies have identified non-marine sources for the phytoplankton biomarkers brassicasterol and dinosterol. Brassicasterol has been shown to be associated with either a limnic source in river dominated Arctic shelf regions, for example, the Laptev Sea (Fahl & Stein, 1999; Hörner et al., 2016; Yunker et al., 1995) or a sea-ice source in the Canadian Arctic Archipelago (Belt et al., 2013). Dinosterol, on the other hand, has been identified in melt ponds of Antarctic glaciers (Jungblut et al., 2009). It is thus conceivable that these biomarkers could have been delivered to our core site from sea ice and/or melt ponds/proglacial lakes of the LIS, in addition to their production on the surface ocean by marine phytoplankton.

However, in our sediment record, we do not find any evidence of a sea-ice source of dinosterol based on the absence of a clear correlation with the sea-ice biomarker IP_{25} (and $r^2 = 0.04$, $p < 0.001$) (Figure 5). Brassicasterol however shows slightly elevated correlations with IP_{25} ($r^2 = 0.27$, $p < 0.001$), which may not completely rule out a sea-ice source, as reported by Belt et al. (2013) from the Canadian Arctic. Based on our record, we cannot distinguish further between the sources of brassicasterol. Hence, we will focus on dinosterol as biomarker for open marine productivity.

To test for a non-marine source of brassicasterol and dinosterol, we investigated their relationship with the terrigenous biomarker campesterol, which originates predominantly from land plants.

We find elevated correlations of campesterol with brassicasterol for the entire record ($r^2 = 0.58$, $p < 0.001$), and significantly lower correlations with dinosterol ($r^2 = 0.08$, $p < 0.001$). However, for certain intervals we also find high correlations for dinosterol with campesterol for example, from 9.3 to 8.9 Kyr BP ($r^2 = 0.75$, $p < 0.001$) and 3.5–0 Kyr BP ($r^2 = 0.73$, $p < 0.001$) (for details see Table S3 in Supporting Information S1). This may point to a non-marine source of brassicasterol and during specific time intervals, for dinosterol.

Another explanation for the correlations between terrigenous and open-water phytoplankton biomarkers could be the input of campesterol by sea ice, which fertilized phytoplankton blooms. This has been observed previously by similarly high accumulation of terrigenous sterols and phytoplankton biomarkers in the context of ice-edge and polynya situations due to strong glacial erosion and melting (e.g., Stein et al., 2017a). We find evidence for this

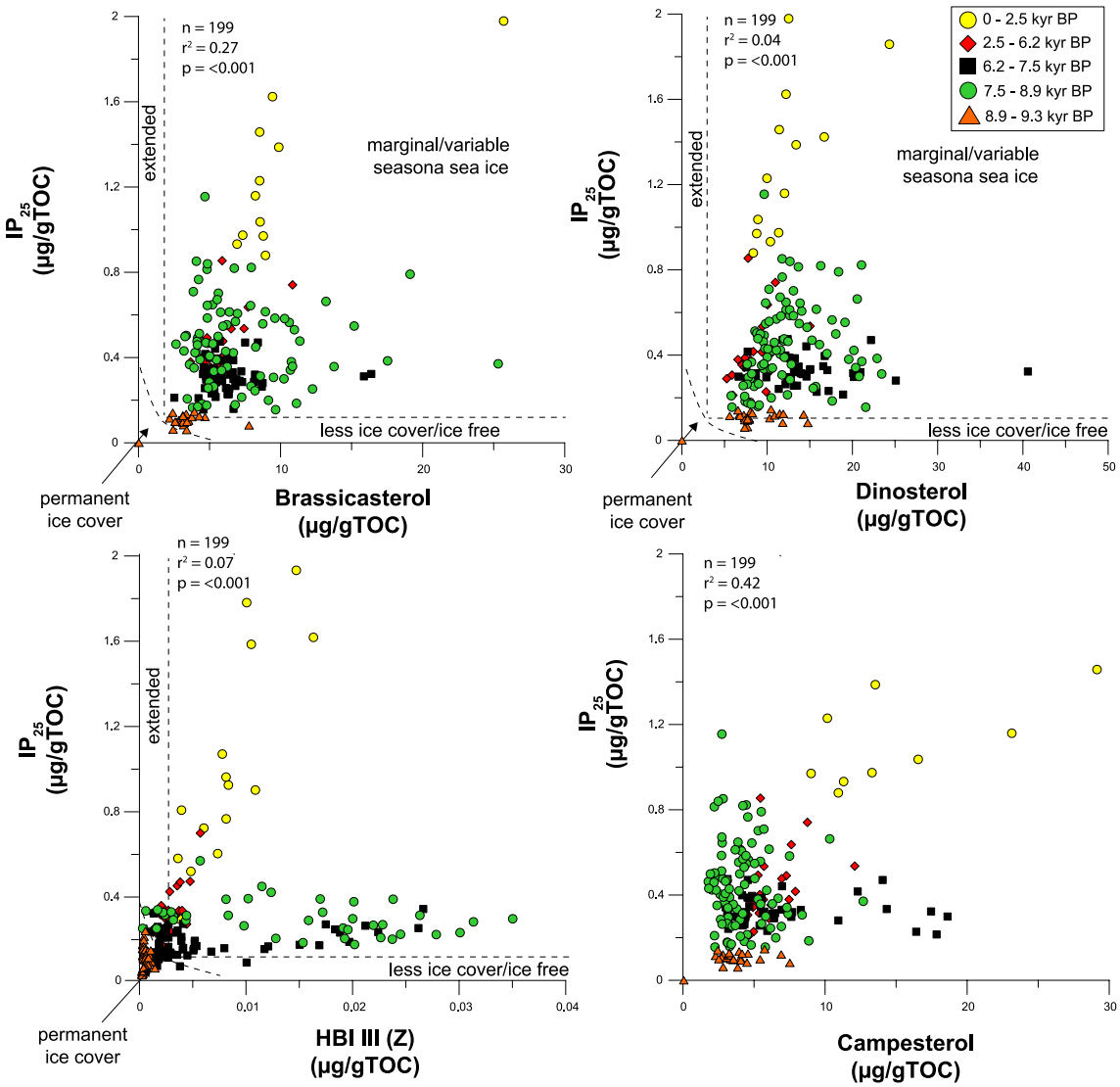

Figure 5. Correlations of brassicasterol, dinosterol, HBI III (Z) and campesterol with IP_{25} (all in µg/gTOC, to circumvent influences of variable TOC on the correlations) for the time intervals 9.3–8.9 Kyr BP (orange triangle), 8.9–7.5 (green circle), 7.5–6.2 (blue square), 6.2–3.5 (red diamond) and 3.5–0 Kyr BP (yellow circle), indicating shifts from extended or ice free to variable seasonal sea ice conditions. Classification of sea-ice scenarios after Müller et al. (2011).

scenario in our record that is, slightly elevated correlations between IP_{25} and campesterol ($r^2 = 0.42$, $p < 0.001$, Table S5 in Supporting Information S1). Further, our sea-ice biomarker record indicates the presence of sea ice and in some cases the presence of an active ice edge during periods of high correlation between dinosterol and campesterol. Glacial erosion and/or dirty sea ice originating from Hudson Bay or the Labrador coast could be an explanation for the relationship of those biomarkers without an allochthonous source of brassicasterol and dinosterol.

In summary, we recommend caution using brassicasterol and dinosterol as single indicators of phytoplankton productivity. However, the observed correlations seem to support the input of terrigenous material and associated biomarkers by sea ice, which in turn may have supported phytoplankton blooms. In the following we will mainly focus on dinosterol, the phytoplankton biomarker which shows the lowest correlations to the terrigenous sterol campesterol and the sea ice biomarker IP_{25} for the overall record. To prevent false interpretation of dinosterol signals we interpret them together with BSi and TOC as indicators for marine productivity.

BSi is another indicator of phytoplankton (diatom) productivity (e.g., Nelson et al., 1999; Ragueneau et al., 2000; Stein et al., 2017b). For this proxy, we do not find a correlation to either the sea-ice biomarker IP_{25} or the

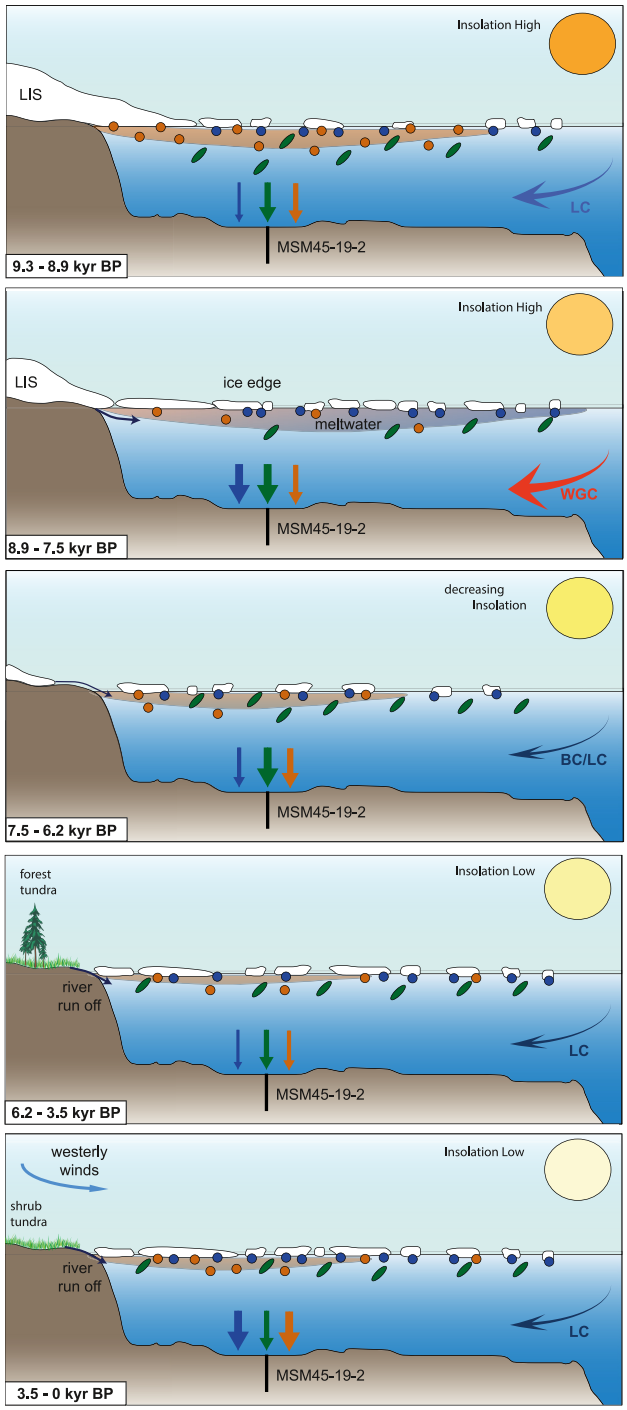

Figure 6. Schematic cross-section (W–E) of the Labrador Shelf at 58°N showing the production areas of sea-ice biomarkers (blue) phytoplankton biomarkers (green ovals), and the input of suspended matter (brown areas) carrying terrigenous sterols (orange) during five different intervals during the past 9.3 Kyr. The blue, green and orange arrows indicate the accumulation of sea ice, open water phytoplankton and terrigenous biomarkers, respectively. Dominant currents are indicated by blue (LC, Labrador Current; BC, Baffin Current) and red (WGC, West Greenland Current) arrows. Size of arrows indicates current influence (strength). Vegetation after Harrison et al. (2013).

terrigenous sterol campesterol (r^2 = 0.24, 0.23; Figure 4, Table S6a in Supporting Information S1). Based on the slight correlation of BSi and TOC (r^2 = 0.70; Table S6 in Supporting Information S1), we assume that TOC concentrations are mostly driven by marine productivity. Furthermore, we find no clear correlation between brassicasterol and BSi (r^2 = 0.24; Table S6a in Supporting Information S1). This supports findings of Dubois et al. (2010), who also find no strict relationship between sedimentary opal and brassicasterol concentrations. They suggest either a change in diatom assemblages, or different sedimentary preservation of BSi and brassicasterol, which could both explain our findings.

Together, the above considerations caution the interpretation of individual indicators for marine productivity and we will consider the combination of all indicators for open water marine phytoplankton productivity at our core site.

4.2. Semi-Quantitative Sea-Ice Reconstructions

The phytoplankton marker HBI III (Z) is considered a more specific marine phytoplankton marker and has been used for the calculation of the $P_{III}IP_{25}$ index (Belt et al., 2015; Smik et al., 2016). One of the main advantages of HBI III (Z) as phytoplankton biomarker used in the calculation of the PIP_{25} index is the similar concentrations with IP_{25}, which made the use of the balance factor *c* dispensable for the Barents Sea (Belt et al., 2015; Smik et al., 2016). However, our record from the Labrador Shelf displays larger concentration differences between IP_{25} and HBI III (Z), which results in a *c* factor of 0.2862 (Figure 4, Figure S2 in Supporting Information S1). Additionally, the source of HBI III (Z) is not yet completely established (Belt et al., 2017; Rowland et al., 2001) and the relationship between HBI III (Z), IP_{25} and sea-ice concentration has only been studied in a few samples from the Labrador Shelf (Kolling et al., 2020). All prior studies focus on more Arctic settings (Belt et al., 2015; Köseoğlu et al., 2018; Ribeiro et al., 2017; Smik & Belt, 2017; Smik et al., 2016). Further, Saini et al. (2020) have associated periodic and high peaks in HBI III (Z), as observed in our core, with phytoplankton blooms linked with wind induced upwelling in ice-edge/polynya environments during winter months. Hence, HBI III (Z) may represent a very specific scenario in our study region that may not be suitable to contribute to a more general sea-ice reconstruction. Based on this, the $P_{III}IP_{25}$ index of our record has to be viewed with caution, especially concerning semi-quantitative sea-ice reconstructions.

With respect to the uncertainties of the producers and the exact ecology of HBI III (Z) and the possible non-marine source of brassicasterol (see Section 4.1), we consider the P_DIP_{25} index to be the most reliable. However, the exact interpretation for sea-ice conditions remains difficult in the absence of larger surface data sets. We will proceed with caution in its interpretation and use it only in combination with the concentrations/accumulation rates of the investigated biomarkers for sea ice and phytoplankton productivity.

Despite these caveats, we find our records to be consistent with previous paleoceanographic reconstructions, specifically sea-ice and WGC reconstructions in the Labrador region (e.g., Limoges et al., 2020; Saini et al., 2020; You et al., 2023) (Figure 6). These will be discussed in Section 4.3.

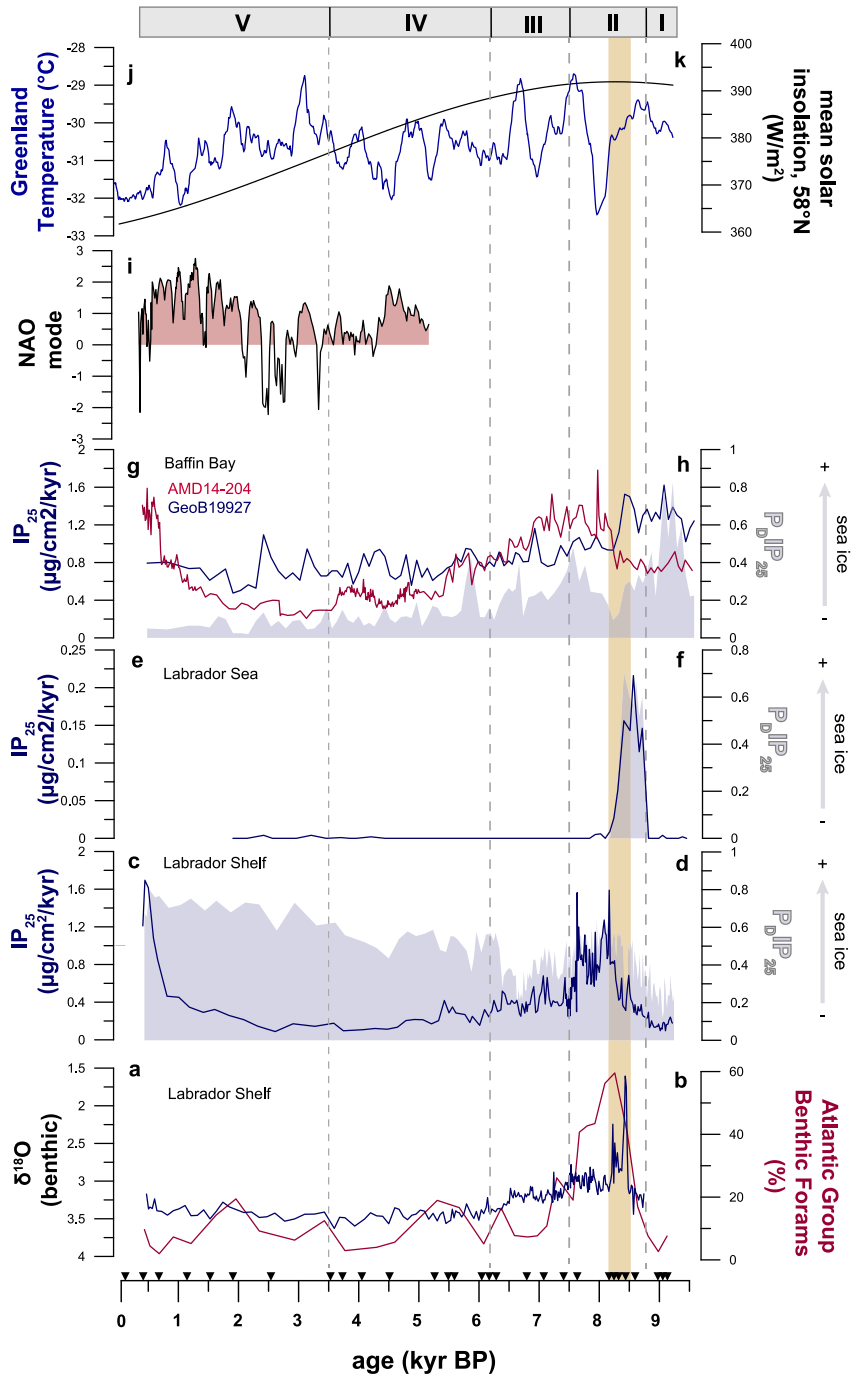

Figure 7. Comparison of different proxies from the Labrador Shelf, Labrador Sea and Baffin Bay against age (Kyr BP). (a) Stable benthic oxygen isotopes $\delta^{18}O$ (Lochte et al., 2019a), (b) Atlantic group of benthic foraminifera (adapted from Lochte et al., 2019b), (c) IP_{25} accumulation rates (in µg/cm^2/Kyr) and (d) P_DIP_{25} index (this study) all from the Labrador Shelf. (e) IP_{25} accumulation rates (in µg/cm^2/Kyr) and (f) P_DIP_{25} index from the NW Labrador Sea (You et al., 2023). (g) IP_{25} accumulation rates (in µg/cm^2/Kyr) and (h) P_DIP_{25} index from the NE Baffin Bay (Limoges et al., 2020; Saini et al., 2020). (i) NAO reconstructions (Olsen et al., 2012), (j) Greenland temperatures from GISP ice core (Alley et al., 2010) and (k) mean solar insolation at 58°N (Laskar et al., 2004). The vertical yellow bar indicates the period of maximum meltwater outflow from the Laurentide Ice Sheet toward the study area. Roman numerals indicate the different climate intervals identified on the Labrador Shelf.

4.3. Environmental Conditions on the Labrador Shelf

4.3.1. Interval I: 9.3–8.9 Kyr BP

Minimum sea-ice conditions are indicated by relatively low concentrations of the sea-ice productivity marker IP_{25} from 9.3 to 8.9 Kyr BP (Figure 4). In combination with intermediate concentrations of the phytoplankton marker dinosterol, the sea-ice index P_DIP_{25} indicates lower than modern sea-ice conditions (Figures 5 and 7). This is in line with previous studies from the Labrador Sea, inferring a retreat of perennial sea ice during this time interval (Gibb et al., 2015; Saini et al., 2022).

We note that benthic foraminiferal assemblages have been interpreted to indicate strong subsurface polar/LC inflow and nearly perennial sea-ice cover at our core site (Lochte et al., 2019b), which differs from our biomarker records in the same sediment core. However, benthic foraminifera are not necessarily a direct indicator for sea ice (Seidenkrantz, 2013), and the more direct sea-ice proxy IP_{25} is thought to provide a more reliable signal. Reconstructions based on IP_{25} and dinocysts, from the northwestern and northeastern Labrador Sea, also indicate a reduction in sea ice during this period (Gibb et al., 2015; Saini et al., 2020; You et al., 2023). These findings support our interpretation, however they do not rule out a strong LC and polar water inflow, as indicated by benthic foraminifera (Lochte et al., 2019b). The combination of reduced sea ice in a major sea ice source area for the Labrador Shelf and an increased LC strength, may explain our observations.

Intermediate concentrations of the terrigenous sterol campesterol during this period (Figure 4) may point to relatively high input of terrigenous material from the adjacent glaciers, that is, Laurentide, Inuitian and Greenland Ice Sheets. High concentrations of $\%C_{37:4}$ support this interpretation, as high amounts of $\%C_{37:4}$ have been inferred to be an indicator of strong meltwater input (Lochte et al., 2019a, and references therein). Similarly, strong meltwater input has been found by other studies from the Labrador Sea during this time interval (e.g., Andrews et al., 1999).

For the time interval between 9.3 and 8.9 Kyr BP, we observe intermediate to high accumulation of proxies associated with open water phytoplankton productivity (e.g., TOC, BSi, Figure 3; dinosterol, brassicasterol, Figure 4). The minimum sea-ice conditions seem to have favored phytoplankton productivity, which probably benefited from high nutrient availability in the photic zone stemming from high terrigenous input. This could also explain the high correlations between terrigenous and phytoplankton biomarkers, and would, in fact, support the marine origin of brassicasterol and dinosterol (see Section 4.1).

In summary, between 9.3 and 8.9 Kyr BP, the core location on the northwestern Labrador shelf was influenced by low/variable seasonal sea-ice cover and high terrigenous input from the surrounding glaciers. This in turn, appears to have promoted phytoplankton productivity (Figure 6).

4.3.2. Interval II: 8.9–7.5 Kyr BP

Interval II, between 8.9 and 7.5 Kyr BP, is characterized by rising IP_{25} concentrations which indicate increased sea-ice algae productivity and thus an increase in seasonal sea ice (Figures 4 and 6). This increase of sea ice occurs at the same time as a strengthened inflow of Atlantic water (Figures 6 and 7; Lochte et al., 2019a), supplying more Atlantic water toward the inner LC (e.g., Lochte et al., 2019a, 2019b; Yang & Piper, 2021). This in turn seems to have promoted subglacial melting which led to the initial Lake Agassiz-Ojibway outburst around 8.5 Kyr BP and the meltwater spike associated with the Hudson Bay Ice Saddle collapse around 8.5 Kyr BP, identified by a strong reduction in $\delta^{18}O$ (Lochte et al., 2019a). With increasing Atlantic water inflow, meltwater input toward the Labrador Shelf increased, which led to reduced surface salinity that may have gradually promoted sea-ice formation (e.g., Close et al., 2018) as indicated in our record. These findings are supported by abrupt increases in sea ice during meltwater intrusions and sea surface temperature (SST) reductions between 8.74 and 8.33 Kyr BP in the northwestern Labrador Sea (Figure 7; You et al., 2023).

During the interval from 8.9 to 7.5 Kyr BP, our record indicates a slight increase in terrigenous input and open water productivity (Figures 3 and 4). However, we observe strong fluctuations in the phytoplankton biomarkers, indicating a variable environment. Probably strong inflow of freshwater during this event created at times a nutrient-depleted freshwater lens, causing surface cooling and increased stratification, hampering most biogenic productivity. This is especially evident in the sedimentation rates, which show a large drop around 8.3 Kyr BP (Figure 3). During other times, higher terrigenous input may have favored phytoplankton blooms. The influence of freshwater and the subsequent (seasonal) stratification of the water column and its effect on different

phytoplankton species in the modern ocean has been discussed in several recent studies (e.g., Mathis & Mikolajewicz, 2020; von Appen et al., 2021). The stronger increase in sea-ice algae compared to phytoplankton productivity leads to a rise in the P_DIP_{25} index, supporting the extension of seasonal sea-ice cover (Figures 5 and 7). The maximum sea-ice extent seems to have been reached between 8.4 and 8.0 Kyr BP (Figure 7), which correlates with the meltwater peak associated with the final outburst from the Lake Agassiz-Ojibway and Hudson Bay Ice Saddle collapse around 8.5 Kyr BP (Lochte et al., 2019a). The influence of the meltwater outburst is also recognized in sea ice increases in the northeastern Labrador Sea (Figure 7; You et al., 2023).

From 8.2 Kyr BP onwards, high concentrations of IP_{25} and HBI III (Z) (Figure 4) indicate the establishment of a stable early spring ice edge at the core location on the northern Labrador shelf. The resulting local nutrient upwelling, which is generally associated with ice-edge conditions (Sakshaug, 2004), may have promoted phytoplankton productivity, indicated by a slight rise in phytoplankton indicators (Figures 3 and 4). Continued strong meltwater influence during this interval, as seen in high concentrations of $\%C_{37:4}$ and low $\delta^{18}O$ values (Lochte et al., 2019a; Figure 7), supports the interpretation of ongoing high freshwater input. Another process that could account for the high HBI III (Z) concentrations during this period is enhanced sea-ice drift, which has been observed during the opening in Kennedy Channel in Nares Strait (Georgiadis et al., 2020). Whether the high HBI III (Z) concentrations are caused by an ice edge or drift ice pulses or a combination of both is difficult to distinguish based on our record.

The increases in sea ice and the establishment of an ice edge over the core site coincide with the widespread 8.2 Kyr BP cold event caused by a major disruption in the AMOC due to massive meltwater inflow (Ellison et al., 2006; Kleiven et al., 2008). It seems that the atmospheric cooling followed the meltwater peak (Figure 7; Lochte et al., 2019a) and the increases in sea ice on the Labrador Shelf and the Labrador Sea (Figure 7; You et al., 2023). This may either be related to uncertainties in age models, that is, reservoir corrections, or by a time lag between ocean circulation and atmospheric temperatures (Muschitiello et al., 2019).

To summarize, interval II is characterized by increasing seasonal sea ice, promoted by reduced salinities following the large freshwater outbursts from the disintegrating LIS, which caused a widespread atmospheric cooling (Figure 7) (Barber et al., 1999; Ellison et al., 2006; Oster et al., 2017; Park et al., 2019; Thomas et al., 2007; Wiersma & Renssen, 2006; Yu et al., 2010). High freshwater input seems to have created a variable environment for phytoplankton productivity, which shifted between nutrient-depleted freshwater and terrigenous input carrying nutrients (Figures 4 and 6).

4.3.3. Interval III: 7.5–6.2 Kyr BP

Following the abrupt freshwater and cooling events between 8.5 and 8.2 Kyr BP, IP_{25} concentrations decreased, indicating a reduction in sea ice diatom productivity, around 7.5 Kyr BP (Figure 4). Open water phytoplankton productivity remains variable but relatively high (Figure 4). The active sea-ice margin that prevailed previously over the core site likely moved further north, as indicated by continuously decreasing IP_{25} and nearly absent HBI III (Z) accumulation (Figure 4). Sea ice and phytoplankton biomarkers combined in the P_DIP_{25} index indicate intermediate sea ice concentrations, which may be representative of low seasonal sea ice conditions (Figure 7). These findings agree with sea-ice records from eastern Baffin Bay and northwestern Labrador Sea where reduced seasonal sea-ice conditions to ice free conditions are observed from 7.75 Kyr BP to 8 Kyr BP, respectively, onwards (Figure 7; Saini et al., 2020; You et al., 2023). The reduction in seasonal sea ice can be associated with the Holocene Thermal Maximum (HTM), which is generally associated with high northern hemisphere summer insolation (Figure 7), along with a decreasing influence of meltwater due to the advanced deglaciation of the Labrador Ice Dome during this period (Dalton et al., 2020). The HTM has been observed in northeast Canada from 8.5 Kyr BP onwards by increasing atmospheric temperatures (Kaufman et al., 2004). Further, the HTM has been characterized by a reduced inflow of Atlantic waters and an increasing influence of the cold Baffin Current (BC) toward the inner LC, as inferred from benthic foraminiferal assemblages (Figure 7) (Lochte et al., 2019b). In combination with decreasing sea-ice conditions in Baffin Bay (Figure 7) (Limoges et al., 2020; Saini et al., 2020) and Labrador Sea (Gibb et al., 2015), the increased inflow of polar waters may have resulted in decreased advection of sea ice to our core site.

Terrigenous input, as inferred from campesterol concentrations, remains relatively high during interval III (Figure 4). This trend can be linked to the remaining ice sheets on Labrador (Dalton et al., 2020; Rashid et al., 2017) and increasing vegetation on newly deglaciated areas around for example, lake Hebron (Lamb, 1984).

These appear to be small and local signals that affected only the Labrador Shelf, as other records from the northeastern Labrador Sea do not record any meltwater pulses (You et al., 2023).

Phytoplankton productivity remains highly variable, which may be related to enhanced primary productivity inferred from benthic foraminiferal assemblages at our core site (Lochte et al., 2019b). However, a drop in dinosterol concentrations around 6.4 Kyr BP is observed, which could point toward a reduction in phytoplankton productivity (Figure 4). A reduction of phytoplankton productivity, in turn, is consistent with findings from the northwest Labrador Sea, where dinocyst reconstructions revealed a general decrease in annual productivity from ca. 7 Kyr BP onwards. This trend is accompanied by weaker stratification due to reduced meltwater inflow and a shift to warmer winter but colder summer SSTs (Gibb et al., 2014).

In summary, interval III (7.5–6.2 Kyr BP) can be associated with the onset of the HTM, with low seasonal sea-ice conditions and variable, high terrigenous input, due to the remaining glaciers in the hinterland (Figure 6). Phytoplankton productivity could benefit from both more open sea-ice conditions and nutrient input from terrigenous sources (Figure 6).

4.3.4. Interval IV: 6.2–3.5 Kyr BP

Relatively low IP_{25} concentrations between 6.2 and 4.3 Kyr BP indicate a phase of low sea-ice algae productivity followed by a slight increase after 4.3 Kyr BP (Figure 4). Following a brief phase of low phytoplankton productivity, based on brassicasterol and dinosterol concentrations, phytoplankton productivity is increasing slightly and remains at intermediate levels (Figure 4). TOC and BSi indicate relatively high productivity with significant variability during this period (Figure 3). Further, accumulation rates and concentrations of the biomarkers do not show a parallel trend, which may indicate a shift in sedimentation regime.

The combination of IP_{25} and dinosterol results in a relatively high P_DIP_{25} index (Figure 7), indicating high seasonal sea-ice conditions on the Labrador Shelf for this interval. Based on the parallel decrease of sea-ice and phytoplankton biomarkers, we assume sea-ice conditions became harsher than in the previous interval III (Figure 6).

On the one hand, relatively warm conditions, associated with the HTM, have been found for the interval between 6.2 and 3 Kyr BP, air temperatures over Greenland remain relatively warm (Figure 7; Alley et al., 2010), warm SSTs are also reported from Baffin Bay (Allan et al., 2021; Levac, 2001) and sea ice is reported to decrease in eastern Baffin Bay (Saini et al., 2022). On the other hand, our findings indicate a cooling and increased seasonal sea ice, based on IP_{25} concentrations, on the Labrador Shelf. This is supported by findings of freshening and cooling of the inner LC due to high melting in the Arctic and increases in meltwater export toward the Labrador Sea. This, in turn seems to have stabilized the surface waters and favored winter cooling and sea-ice growth (Deser, 2002; Solignac et al., 2011). This cooling is also evidenced by decreasing subsurface water temperatures in core MSM45-19_2 between 6.2 and 5.6 Kyr BP (Lochte et al., 2019b) and also by increases in sea ice and decreases in SSTs off Newfoundland (Richerol et al., 2016; Sheldon et al., 2016). We assume that a strong inner LC, which has been influenced by a strong BC (polar outflow via western Baffin Bay) (Lochte et al., 2019b) and a WGC (Atlantic inflow along eastern Baffin Bay), affected by strong inflow of Atlantic Intermediate Water (Jennings et al., 2002), caused the opposing signals in the east (eastern Baffin Bay) and west (Canadian Shelf).

It should be noted that some records from more southern locations on the eastern Canadian Shelf also indicate a warming period between ca. 5.6 and 3.5 Kyr BP (e.g., Lochte et al., 2020; Sheldon et al., 2016) associated with the HTM (Kaufmann et al., 2004). Cléroux et al. (2008) assumed that the LC did not reach their core site off North Carolina and that a northward displacement of the Gulf Stream created a warming trend. In our record, we do not see a clear indication of warming. IP_{25} and dinosterol concentrations are relatively low during this period (Figure 4). In contrast, TOC concentrations as well as benthic foraminifera (Lochte et al., 2019b) indicate a high productivity phase (Figure 3). A stronger influence of Gulf Stream-derived water should result in a clear warming, indicated by all proxies. We assume that the signal recorded in the records further south did not reach or affect the core site on the Labrador Shelf. The northwestern Labrador Shelf seems to be mainly influenced by a strong inner LC and the reduction of the solar insolation and the onset of the Neoglacial cooling which commenced at ca. 4–5 Kyr BP in northeast Canada with a series of glacial readvances (Andrews et al., 1999; Andrews & Tedesco, 1992; Davis & Jacobson, 1985). However, the stronger Gulf Stream will subsequently affect the NAC and IrC feeding into the WGC, which could account for warmer signals found in the eastern Baffin Bay records (described above).

Terrigenous sterols on the Labrador Shelf show one final peak at ca. 5.5 Kyr BP, which may be related to the disappearance of the last glaciers in Labrador (Dalton et al., 2020). Following this peak sterol concentrations show a decreasing trend, indicating that terrigenous input was relatively low during interval IV (Figure 3).

4.3.5. Interval V: 3.5–0 Kyr BP

The increasing trend in seasonal sea ice, indicated by rising IP_{25} concentrations and P_DIP_{25} values, continues and becomes more apparent during the past 3.5 Kyr (Figures 5 and 7). We assume sea ice remained seasonal and without the formation of an ice edge in the proximity to the core site, as HBI III (Z) accumulation and concentration remain at low levels (Figure 4). This increase in seasonal sea ice on the Labrador Shelf is associated with the Neoglacial cooling trend, linked to declining solar insolation (Figure 7). Our findings agree with results from the northwest Labrador Sea, where dinocyst-based reconstructions indicate colder, less saline sea surface conditions with increased ice cover after 2 Kyr BP (Gibb et al., 2014).

We assume that this increase in sea ice is associated with a prevailing positive mode of the NAO during the Neoglaciation (Figure 7; Olsen et al., 2012). The positive NAO mode is associated with stronger northwesterly winds that carry Arctic air and/or low salinity and temperature anomalies to the study area, favoring the formation of local sea ice (Deser, 2002; Drinkwater, 1996; Petrie, 2007; Prinsenberg et al., 1997). However, the positive mode of the NAO is also associated with a stronger AMOC resulting in an increased northward advection of Atlantic waters toward the north (e.g., Trouet et al., 2009). However, during this interval, a re-occurrence of polar waters from the BC has been reported from Labrador Shelf and Sea (Gibb et al., 2015; Lochte et al., 2019b). Strong westerly winds, caused by the positive NAO, may have caused an eastward shift in the Irminger Current, carrying Atlantic waters north, to make way for the southward flowing waters of the BC, carrying cold and ice laden waters to the core site on the Labrador Shelf. Due to the low resolution of the late Holocene in our core, further interpretation on the influence of the NAO on sea ice on the Labrador Shelf is not possible.

In addition to influences of the NAO mode, sea ice may also be exported from the now open Canadian Arctic (Knudsen et al., 2008), one of the two export routes of Arctic sea ice into the North Atlantic. The latter is supported by evidence for a persistent Canadian archipelago source in the LC during the past 1.6 Kyr BP (Keigwin et al., 2003) and increases in sea ice in Disko Bugt during the past 2.2 Kyr BP (Kolling et al., 2018; Krawczyk et al., 2013), and Baffin Bay during the past 3 Kyr BP (Limoges et al., 2020; Saini et al., 2022; Figure 7). All of these may lead to an enhanced sea-ice export to the Labrador Shelf.

Terrigenous input increased sharply during the past 2 Kyr, based on campesterol concentrations (Figure 4). This trend may be related to the opening of the forest tundra and fire occurrence observed in Northern Quebec during this interval (Asselin & Payette, 2005), which could have increased the terrigenous material transported toward our core site via Hudson Bay.

The Neoglacial cooling observed at our core site seems to have affected different phytoplankton producers differently. TOC, BSi and the phytoplankton biomarkers brassicasterol and dinosterol rise slightly (Figures 3 and 4; this study). Benthic foraminiferal productivity shows no change or a minor increase, and alkenone concentrations decrease during this interval (Lochte et al., 2019b). We assume that reduced stratification during this interval (Solignac et al., 2004) provided at times favorable environmental conditions for some phytoplankton species during the ice-free late spring/summer whereas other groups struggled with the high inflow of nutrient-poor and cold polar water masses (e.g., Gibb et al., 2015; Lochte et al., 2019b; Müller et al., 2012). The phytoplankton community on the Labrador Shelf is dominated by different species, depending on the season, diatoms dominate the phytoplankton community during spring, dinoflagellates throughout autumn/winter (Harrison et al., 2013). More detailed studies from Baffin Bay reveal similar results (Jensen & Christensen, 2014), and additionally indicate the dominance of haptophytes during late winter/early spring. A similar seasonal shift in phytoplankton community on the northern Labrador Shelf could explain the reduction in alkenone concentrations, produced by haptophytes which seem to bloom during the still ice-covered late winter/early spring, which would hamper the haptophyte bloom. Furthermore, diatoms and dinoflagellates could benefit from the ice-free conditions and nutrient availability during the (nearly) ice-free spring and autumn. This in turn could have increased the export of organic matter toward the sea floor, indicated by rising TOC concentrations (Figure 3), which would have provided a food source for benthic foraminifera.

In summary, interval V is characterized by an increase in seasonal sea ice following the Neoglacial cooling. Terrigenous input increased due to vegetation changes in the hinterland, which provided nutrients for phytoplankton communities blooming during the ice-free season in late spring, summer and autumn (Figure 6).

5. Conclusions

Sea-ice conditions and phytoplankton productivity on the northwestern Labrador Shelf over the last 9.3 Kyr were reconstructed based on geochemical and bulk sedimentary proxies in a well dated sediment core (MSM45_19-2).

With this approach, we identified five intervals:

1. Between 8.9 and 8.5 Kyr BP, the Labrador Shelf is characterized by low seasonal sea-ice conditions and the melting of the proximal LIS. High terrigenous input from the LIS and a short sea-ice season seem to have favored phytoplankton productivity.
2. From 8.9 Kyr onwards, increased inflow of warm Atlantic waters triggered the Lake Agassiz-Ojibway drainage and the Hudson Bay Ice Saddle collapse, which caused massive meltwater outbursts toward the North Atlantic between 8.5 and 8.2 Kyr BP. Parallel to the increased meltwater input and subsequent freshening of the surface ocean, sea ice increased toward harsh seasonal sea-ice cover and the formation of an ice edge over the core site. The harsh seasonal sea-ice conditions and high freshwater input seem to have hampered phytoplankton blooms.
3. After the massive freshwater events, the interval between 7.5 and 6.2 Kyr BP was characterized by decreasing sea-ice conditions, a trend which is likely associated with the HTM. Phytoplankton productivity could benefit from the more open sea-ice conditions and a reduction in meltwater. However, terrigenous input was still relatively high, associated with the melting of the last remaining glaciers in the hinterland.
4. During interval IV, 6.2–3.5 Kyr BP, sea-ice conditions seemed to increase slightly and phytoplankton productivity remained at intermediate levels, whereas other records further east still indicate warm HTM conditions. This may be related to a strong and fresh inner LC in the west (Labrador Shelf) and a strong Atlantic inflow in the east (Baffin Bay).
5. Following the Neoglaciation, seasonal sea-ice conditions became harsher after 3.5 Kyr BP. The increase in sea-ice cover may also be associated with a positive mode of the NAO. Different productivity indicators show different signals during this period, possibly indicating a strong seasonality in phytoplankton production.

Data Availability Statement

The radiocarbon age model was implemented in the software package OxCal v4.4.4 (Ramsey, 2008, 2009), using the marine data from Heaton et al. (2020) for calibration (Marine20) (Figure 2). Local marine radiocarbon reservoir offset data was taken from McNeely et al. (2006) and Coulthard et al. (2010). All biomarker data, including concentrations normalized to total organic carbon (µg/gTOC) and gram sediment (µg/gSed) used for this research are available at PANGAEA—Data Publisher for Earth & Environmental Science via Kolling, Doering, et al. (2022) and Kolling et al. (2022a, 2022b) with license Creative Commons Attribution 4.0 International. Bayesian age model code is available at Zenodo (Kolling et al., 2023) with license Creative Commons Attribution 4.0 International.

Acknowledgments

We would like to thank the captain, crew, and the scientific party of the R/V *Maria S. Merian* expedition MSM45. We are very thankful to Walter Luttmer for technical support in the biomarker laboratory. Claire Normandeau assisted with the biogenic opal analysis. We acknowledge funding from the Ocean Frontier Institute (OFI) and NSERC. This manuscript benefitted from three anonymous reviewers and the work of the editor. Open Access funding enabled and organized by Projekt DEAL.

References

Aagaard, K., & Coachman, L. (1968a). The East Greenland current north of Denmark Strait: Part I. *Arctic*, *21*(3), 181–200. https://doi.org/10.14430/arctic3262

Aagaard, K., & Coachman, L. (1968b). The East Greenland current north of Denmark Strait: Part II. *Arctic*, *21*(4), 267–290. https://doi.org/10.14430/arctic3270

Allan, E., de Vernal, A., Seidenkrantz, M. S., Briner, J. P., Hillaire-Marcel, C., Pearce, C., et al. (2021). Insolation vs. meltwater control of productivity and sea surface conditions off SW Greenland during the Holocene. *Boreas*, *50*(3), 631–651. https://doi.org/10.1111/bor.12514

Alley, R. B., Andrews, J. T., Brigham-Grette, J., Clarke, G. K. C., Cuffey, K. M., Fitzpatrick, J. J., et al. (2010). History of the Greenland Ice Sheet: Paleoclimatic insights. *Quaternary Science Reviews*, *29*(15–16), 1728–1756. https://doi.org/10.1016/j.quascirev.2010.02.007

Andrews, J. T., Keigwin, L., Hall, F., & Jennings, A. E. (1999). Abrupt deglaciation events and Holocene palaeoceanography from high-resolution cores, Cartwright Saddle, Labrador Shelf, Canada. *Journal of Quaternary Science*, *14*(5), 383–397. https://doi.org/10.1002/(SICI)1099-1417(199908)14:5<383::AID-JQS464>3.0.CO;2-J

Andrews, J. T., & Tedesco, K. (1992). Detrital carbonate-rich sediments, northwestern Labrador Sea: Implications for ice-sheet dynamics and iceberg rafting (Heinrich) events in the North Atlantic. *Geology*, *20*(12), 1087. https://doi.org/10.1130/0091-7613(1992)020<1087:DCRSNL>2.3.CO;2

Asselin, H., & Payette, S. (2005). Late Holocene opening of the forest tundra landscape in northern Quebec. *Global Ecology and Biogeography*, *14*(4), 307–313. https://doi.org/10.1111/j.1466-822x.2005.00157.x

Bakke, J., Paasche, Ø., Schaefer, J. M., & Timmermann, A. (2021). Long-term demise of sub-Antarctic glaciers modulated by the Southern Hemisphere Westerlies. *Scientific Reports*, *11*(1), 1–10. https://doi.org/10.1038/s41598-021-87317-5

Barber, D. C., Dyke, A., Hillaire-Marcel, C., Jennings, A. E., Andrews, J. T., Kerwin, M. W., et al. (1999). Forcing of the cold event of 8,200 years ago by catastrophic drainage of Laurentide lakes. *Nature*, *400*(6742), 344–348. https://doi.org/10.1038/22504

Belt, S. T. (2019). What do IP25 and related biomarkers really reveal about sea ice change? *Quaternary Science Reviews*, *204*, 216–219. https://doi.org/10.1016/j.quascirev.2018.11.025

Belt, S. T., Allard, W. G., Massé, G., Robert, J. M., & Rowland, S. J. (2000). Highly branched isoprenoids (HBIs): Identification of the most common and abundant sedimentary isomers. *Geochimica et Cosmochimica Acta*, *64*(22), 3839–3851. https://doi.org/10.1016/S0016-7037(00)00464-6

Belt, S. T., Brown, T. A., Ringrose, A. E., Cabedo-Sanz, P., Mundy, C. J., Gosselin, M., & Poulin, M. (2013). Quantitative measurement of the sea ice diatom biomarker IP25 and sterols in Arctic sea ice and underlying sediments: Further considerations for palaeo sea ice reconstruction. *Organic Geochemistry*, *62*(Supplement C), 33–45. https://doi.org/10.1016/j.orggeochem.2013.07.002

Belt, S. T., Brown, T. A., Smik, L., Assmy, P., & Mundy, C. J. (2018). Sterol identification in floating Arctic sea ice algal aggregates and the Antarctic Sea ice diatom *Berkeleya adeliensis*. *Organic Geochemistry*, *118*, 1–3. https://doi.org/10.1016/j.orggeochem.2018.01.008

Belt, S. T., Brown, T. A., Smik, L., Tatarek, A., Wiktor, J., Stowasser, G., et al. (2017). Identification of C25 highly branched isoprenoid (HBI) alkenes in diatoms of the genus Rhizosolenia in polar and sub-polar marine phytoplankton. *Organic Geochemistry*, *110*, 65–72. https://doi.org/10.1016/j.orggeochem.2017.05.007

Belt, S. T., Cabedo-Sanz, P., Smik, L., Navarro-Rodriguez, A., Berben, S. M. P., Knies, J., & Husum, K. (2015). Identification of paleo Arctic winter sea ice limits and the marginal ice zone: Optimised biomarker-based reconstructions of late Quaternary Arctic sea ice. *Earth and Planetary Science Letters*, *431*, 127–139. https://doi.org/10.1016/j.epsl.2015.09.020

Belt, S. T., Massé, G., Rowland, S. J., Poulin, M., Michel, C., & LeBlanc, B. (2007). A novel chemical fossil of palaeo sea ice: IP25. *Organic Geochemistry*, *38*(1), 16–27. https://doi.org/10.1016/j.orggeochem.2006.09.013

Belt, S. T., Smik, L., Köseoğlu, D., Knies, J., & Husum, K. (2019). A novel biomarker-based proxy for the spring phytoplankton bloom in Arctic and sub-arctic settings – HBI T25. *Earth and Planetary Science Letters*, *523*(July), 115703. https://doi.org/10.1016/j.epsl.2019.06.038

Boon, J. J., Rijpstra, W. I. C., de Lange, F., De Leeuw, J. W., Yoshioka, M., & Shimizu, Y. (1979). Black Sea sterol—A molecular fossil for dinoflagellate blooms. *Nature*, *277*(5692), 125–127. https://doi.org/10.1038/277125a0

Brown, T. A., Belt, S. T., Tatarek, A., & Mundy, C. J. (2014). Source identification of the Arctic sea ice proxy IP25. *Nature Communications*, *5*(May), 4197. https://doi.org/10.1038/ncomms5197

Carlson, A. E., Anslow, F. S., Obbink, E. A., LeGrande, A. N., Ullman, D. J., & Licciardi, J. M. (2009). Surface-melt driven Laurentide Ice Sheet retreat during the early Holocene. *Geophysical Research Letters*, *36*(24), L24502. https://doi.org/10.1029/2009GL040948

Carlson, A. E., Clark, P. U., Raisbeck, G. M., & Brook, E. J. (2007). Rapid Holocene deglaciation of the Labrador sector of the Laurentide Ice Sheet. *Journal of Climate*, *20*(20), 5126–5133. https://doi.org/10.1175/JCLI4273.1

Cavalieri, D. J., Parkinson, C. L., Gloersen, P., & Zwally, H. J. (1996). *Sea ice concentrations from Nimbus-7 SMMR and DMSP SSM/ISSMIS passive microwave data, Version 1*. NASA National Snow and Ice Data Center Distributed Active Archive Center. https://doi.org/10.5067/8GQ8LZQVL0VL

Clarke, R. A., & Gascard, J.-C. (1983). The formation of Labrador Sea Water. Part I: Large-scale processes. *Journal of Physical Oceanography*, *13*(10), 1764–1778. https://doi.org/10.1175/1520-0485(1983)013<1764:tfolsw>2.0.co;2

Cléroux, C., Cortijo, E., Anand, P., Labeyrie, L., Bassinot, F., Caillon, N., & Duplessy, J. C. (2008). Mg/Ca and Sr/Ca ratios in planktonic foraminifera: Proxies for upper water column temperature reconstruction. *Paleoceanography*, *23*(3), PA3214. https://doi.org/10.1029/2007PA001505

Close, S., Herbaut, C., Houssais, M. N., & Blaizot, A. C. (2018). Mechanisms of interannual-to decadal-scale winter Labrador Sea ice variability. *Climate Dynamics*, *51*(7), 2485–2508. https://doi.org/10.1007/s00382-017-4024-z

Coulthard, R. D., Furze, M. F. A., Pieńkowski, A. J., Chantel Nixon, F., & England, J. H. (2010). New marine ΔR values for Arctic Canada. *Quaternary Geochronology*, *5*(4), 419–434. https://doi.org/10.1016/j.quageo.2010.03.002

Cronin, T. M., Polyak, L., Reed, D., Kandiano, E. S., Marzen, R. E., & Council, E. A. (2013). A 600-ka Arctic sea-ice record from Mendeleev Ridge based on ostracodes. *Quaternary Science Reviews*, *79*, 157–167. https://doi.org/10.1016/j.quascirev.2012.12.010

Cuny, J., Rhines, P. B., Niiler, P. P., & Bacon, S. (2002). Labrador Sea boundary currents and the fate of the Irminger Sea water. *Journal of Physical Oceanography*, *32*(2), 627–647. https://doi.org/10.1175/1520-0485(2002)032<0627:LSBCAT>2.0.CO;2

Cyr, F., Snook, S., Bishop, C., Galbraith, P. S., Pye, B., Chen, N., & Han, G. (2021). Physical oceanographic conditions on the Newfoundland and Labrador shelf during 2019 (pp. iv+52). DFO Can. Sci. Advis. Sec. Res. Doc., 2021/017(March). Retrieved from http://waves-vagues.dfo-mpo.gc.ca/Library/362068.pdf

Czaja, A., & Frankignoul, C. (2002). Observed impact of Atlantic SST anomalies on the North Atlantic oscillation. *Journal of Climate*, *15*(6), 606–623. https://doi.org/10.1175/1520-0442(2002)015<0606:OIOASA>2.0.CO;2

Dalton, A. S., Margold, M., Stokes, C. R., Tarasov, L., Dyke, A. S., Adams, R. S., et al. (2020). An updated radiocarbon-based ice margin chronology for the last deglaciation of the North American Ice Sheet Complex. *Quaternary Science Reviews*, *234*, 106223. https://doi.org/10.1016/j.quascirev.2020.106223

Davidson, L. W. (1985). *The ice climatology of the Newfoundland Bays* (p. 602). Seaconsult Ltd. Prepared for the Department of Development & Tourism, Physical Planning Speciality Team, Government of Newfoundland and Labrador.

Davis, R. B., & Jacobson, G. L. (1985). Late glacial and early Holocene Landscapes in northern New England and adjacent areas of Canada. *Quaternary Research*, *23*(3), 341–368. https://doi.org/10.1016/0033-5894(85)90040-7

Deser, C. (2002). On the physical nature of the Arctic Oscillation. *Geophysical Research Letters*, *29*(16), 779–782. https://doi.org/10.1029/2002GL015208

de Vernal, A., Gersonde, R., Goosse, H., Seidenkrantz, M. S., & Wolff, E. W. (2013). Sea ice in the paleoclimate system: The challenge of reconstructing sea ice from proxies - An introduction. *Quaternary Science Reviews*, *79*, 1–8. https://doi.org/10.1016/j.quascirev.2013.08.009

de Vernal, A., Henry, M., Matthiessen, J., Mudie, P. J., Rochon, A., Boessenkool, K. P., et al. (2001). Dinoflagellate cyst assemblages as tracers of sea-surface conditions in the northern North Atlantic, Arctic and sub-Arctic seas: The new 'n = 677' data base and its application for quantitative palaeoceanographic reconstruction. *Journal of Quaternary Science*, *16*(7), 681–698. https://doi.org/10.1002/jqs.659

Dickson, B., Dye, S., Jónsson, S., Köhl, A., Macrander, A., Marnela, M., et al. (2008). The overflow flux west of Iceland: Variability, origins and forcing. In *Arctic--Subarctic Ocean fluxes: Defining the role of the northern seas in climate*.

Drinkwater, K. F. (1996). Atmospheric and oceanic variability in the northwest Atlantic during the 1980s and early 1990s. *Journal of Northwest Atlantic Fishery Science*, *18*, 77–97. https://doi.org/10.2960/J.v18.a6

Dubois, N., Kienast, M., Kienast, S., Calvert, S. E., François, R., & Anderson, R. F. (2010). Sedimentary opal records in the eastern equatorial Pacific: It is not all about leakage. *Global Biogeochemical Cycles*, *24*(4), GB4020. https://doi.org/10.1029/2010GB003821

Ellison, C. R. W., Chapman, M. R., & Hall, I. R. (2006). Surface and deep ocean interactions during the cold climate event 8200 years ago. *Science*, *312*(5782), 1929–1932. https://doi.org/10.1126/science.1127213

Fahl, K., & Stein, R. (1997). Modern organic carbon deposition in the Laptev Sea and the adjacent continental slope: Surface water productivity vs. terrigenous input. *Organic Geochemistry*, *26*(5–6), 379–390. https://doi.org/10.1016/s0146-6380(97)00007-7

Fahl, K., & Stein, R. (1999). Biomarkers as organic-carbon-source and environmental indicators in the late quaternary Arctic Ocean: Problems and perspectives. *Marine Chemistry*, *63*(3–4), 293–309. https://doi.org/10.1016/S0304-4203(98)00068-1

Fahl, K., & Stein, R. (2007). Biomarker records, organic carbon accumulation, and river discharge in the Holocene southern Kara Sea (Arctic Ocean). *Geo-Marine Letters*, *27*(1), 13–25. https://doi.org/10.1007/s00367-006-0049-8

Fahl, K., & Stein, R. (2012). Modern seasonal variability and deglacial/Holocene change of central Arctic Ocean sea-ice cover: New insights from biomarker proxy records. *Earth and Planetary Science Letters*, *351*(352), 123–133. https://doi.org/10.1016/j.epsl.2012.07.009

Fratantoni, P. S., & McCartney, M. S. (2010). Freshwater export from the Labrador Current to the North Atlantic Current at the Tail of the Grand Banks of Newfoundland. *Deep-Sea Research Part I: Oceanographic Research Papers*, *57*(2), 258–283. https://doi.org/10.1016/j.dsr.2009.11.006

Georgiadis, E., Giraudeau, J., Jennings, A., Limoges, A., Jackson, R., Ribeiro, S., & Massé, G. (2020). Local and regional controls on Holocene sea ice dynamics and oceanography in Nares Strait, Northwest Greenland. *Marine Geology*, *422*, 106115. https://doi.org/10.1016/j.margeo.2020.106115

Gibb, O. T., Hillaire-Marcel, C., & de Vernal, A. (2014). Oceanographic regimes in the northwest Labrador Sea since Marine Isotope Stage 3 based on dinocyst and stable isotope proxy records. *Quaternary Science Reviews*, *92*, 269–279. https://doi.org/10.1016/j.quascirev.2013.12.010

Gibb, O. T., Steinhauer, S., Fréchette, B., de Vernal, A., & Hillaire-Marcel, C. (2015). Diachronous evolution of sea surface conditions in the Labrador Sea and Baffin Bay since the last deglaciation. *Holocene*, *25*(12), 1882–1897. https://doi.org/10.1177/0959683615591352

Golledge, N. R., Keller, E. D., Gomez, N., Naughten, K. A., Bernales, J., Trusel, L. D., & Edwards, T. L. (2019). Global environmental consequences of twenty-first-century ice-sheet melt. *Nature*, *566*(7742), 65–72. https://doi.org/10.1038/s41586-019-0889-9

Harrison, W. G., Børsheim, K. Y., Li, W. K., Maillet, G. L., Pepin, P., Sakshaug, E., et al. (2013). Phytoplankton production and growth regulation in the Subarctic North Atlantic: A comparative study of the Labrador Sea-Labrador/Newfoundland shelves and Barents/Norwegian/Greenland seas and shelves. *Progress in Oceanography*, *114*, 26–45. https://doi.org/10.1016/j.pocean.2013.05.003

Heaton, T. J., Köhler, P., Butzin, M., Bard, E., Reimer, R. W., Austin, W. E. N., et al. (2020). Marine20 - The marine radiocarbon age calibration curve (0-55,000 cal BP). *Radiocarbon*, *62*(4), 779–820. https://doi.org/10.1017/RDC.2020.68

Hoffman, J. S., Carlson, A. E., Winsor, K., Klinkhammer, G. P., LeGrande, A. N., Andrews, J. T., & Strasser, J. C. (2012). Linking the 8.2 ka event and its freshwater forcing in the Labrador Sea. *Geophysical Research Letters*, *39*(17), L18703. https://doi.org/10.1029/2012GL053047

Hörner, T., Stein, R., Fahl, K., & Birgel, D. (2016). Post-glacial variability of sea ice cover, river run-off and biological production in the western Laptev Sea (Arctic Ocean) - A high-resolution biomarker study. *Quaternary Science Reviews*, *143*, 133–149. https://doi.org/10.1016/j.quascirev.2016.04.011

Huang, W. Y., & Meinschein, W. G. (1979). Sterols as ecological indicators. *Geochimica et Cosmochimica Acta*, *43*(5), 739–745. https://doi.org/10.1016/0016-7037(79)90257-6

Jennings, A., Andrews, J., Pearce, C., Wilson, L., & Ólfasdótttir, S. (2015). Detrital carbonate peaks on the Labrador shelf, a 13-7ka template for freshwater forcing from the Hudson Strait outlet of the Laurentide Ice Sheet into the subpolar gyre. *Quaternary Science Reviews*, *107*, 62–80. https://doi.org/10.1016/j.quascirev.2014.10.022

Jennings, A., Knudsen, K. L., Hald, M., Hansen, C. V., & Andrews, J. T. (2002). A mid-Holocene shift in Arctic sea-ice variability on the East Greenland Shelf. *The Holocene*, *12*(1), 49–58. https://doi.org/10.1191/0959683602hl519rp

Jensen, L. M., & Christensen, T. R. (2014). *Nuuk ecological research operations* (p. 94). 7th Annual Report. Aarhus University, DCE—Danish Centre for Environment and Energy.

Johns, L., Wraige, E. J., Belt, S. T., Lewis, C. A., Massé, G., Robert, J. M., & Rowland, S. J. (1999). Identification of a C25 highly branched isoprenoid (HBI) diene in Antarctic sediments, Antarctic sea-ice diatoms and cultured diatoms. *Organic Geochemistry*, *30*(11), 1471–1475. https://doi.org/10.1016/S0146-6380(99)00112-6

Jungblut, A. D., Allen, M. A., Burns, B. P., & Neilan, B. A. (2009). Lipid biomarker analysis of cyanobacteria-dominated microbial mats in meltwater ponds on the McMurdo Ice Shelf, Antarctica. *Organic Geochemistry*, *40*(2), 258–269. https://doi.org/10.1016/j.orggeochem.2008.10.002

Kaufman, D. S., Ager, T. A., Anderson, N. J., Anderson, P. M., Andrews, J. T., Bartlein, P. J., et al. (2004). Holocene thermal maximum in the western Arctic (0-180°W). *Quaternary Science Reviews*, *23*(5–6), 529–560. https://doi.org/10.1016/j.quascirev.2003.09.007

Keigwin, L. D., Sachs, J. P., & Rosenthal, Y. (2003). A 1600-year history of the Labrador Current off Nova Scotia. *Climate Dynamics*, *21*(1), 53–62. https://doi.org/10.1007/s00382-003-0316-6

Kerwin, M. W. (1996). A regional stratigraphic isochron (ca. 8000 14C yr B.P.) from final deglaciation of Hudson Strait. *Quaternary Research*, *46*(2), 89–98. https://doi.org/10.1006/qres.1996.0049

Kieke, D., & Yashayaev, I. (2015). Studies of Labrador Sea Water formation and variability in the subpolar North Atlantic in the light of international partnership and collaboration. *Progress in Oceanography*, *132*, 220–232. https://doi.org/10.1016/j.pocean.2014.12.010

Kleiven, H. K. F., Kissel, C., Laj, C., Ninnemann, U. S., Richter, T. O., & Cortijo, E. (2008). Reduced North Atlantic Deep Water coeval with the glacial Lake Agassiz freshwater outburst. *Science*, *319*(5859), 60–64. https://doi.org/10.1126/science.1148924

Klitgaard-Kristensen, D., Sejrup, H. P., Haflidason, H., Johnsen, S., & Spurk, M. (1998). A regional 8200 cal. yr BP cooling event in northwest Europe, induced by final stages of the Laurentide ice-sheet deglaciation? *Journal of Quaternary Science*, *13*(2), 165–169. https://doi.org/10.1002/(sici)1099-1417(199803/04)13:2<165::aid-jqs365>3.0.co;2-#

Knudsen, K. L., Stabell, B., Seidenkrantz, M. S., Eiríksson, J., & Blake, W. (2008). Deglacial and Holocene conditions in northernmost Baffin Bay: Sediments, foraminifera, diatoms and stable isotopes. *Boreas*, *37*(3), 346–376. https://doi.org/10.1111/j.1502-3885.2008.00035.x

Kolling, H. M., Doering, K., Kienast, M., Kienast, S. S., & Schneider, R. R. (2022). Biogenic opal record of gravity core MSM45_19-2 [Dataset]. PANGAEA. https://doi.org/10.1594/PANGAEA.949244

Kolling, H. M., Schneider, R., Gross, F., Kienast, M., Kienast, S., Doering, K., et al. (2023). Code of the Bayesian Age model of core MSM45_19-2 [Software]. Zenodo. https://doi.org/10.5281/zenodo.8247131

Kolling, H. M., Schneider, R. R., Stein, R., & Fahl, K. (2022a). Biomarker concentrations in gravity core MSM45_19-2 [Dataset]. PANGAEA. https://doi.org/10.1594/PANGAEA.949065

Kolling, H. M., Schneider, R. R., Stein, R., & Fahl, K. (2022b). Total organic carbon (TOC) content and dry bulk density (DBD) of gravity core MSM45_19-2 [Dataset]. PANGAEA. https://doi.org/10.1594/PANGAEA.949056

Kolling, H. M., Stein, R., Fahl, K., Perner, K., & Moros, M. (2018). New insights into sea ice changes over the past 2.2 kyr in Disko Bugt, West Greenland. *Arktos*, *4*(1), 11–20. https://doi.org/10.1007/s41063-018-0045-z

Kolling, H. M., Stein, R., Fahl, K., Sadatzki, H., de Vernal, A., & Xiao, X. (2020). Biomarker distributions in (Sub)-Arctic surface sediments and their potential for sea ice reconstructions. *Geochemistry, Geophysics, Geosystems*, *21*(10), e2019GC008629. https://doi.org/10.1029/2019GC008629

Köseoğlu, D., Belt, S. T., Smik, L., Yao, H., Panieri, G., & Knies, J. (2018). Complementary biomarker-based methods for characterising Arctic sea ice conditions: A case study comparison between multivariate analysis and the PIP25index. *Geochimica et Cosmochimica Acta*, *222*, 406–420. https://doi.org/10.1016/j.gca.2017.11.001

Krawczyk, D. W., Witkowski, A., Lloyd, J., Moros, M., Harff, J., & Kuijpers, A. (2013). Late-Holocene diatom derived seasonal variability in hydrological conditions off Disko Bay, West Greenland. *Quaternary Science Reviews*, *67*, 93–104. https://doi.org/10.1016/j.quascirev.2013.01.025

Krawczyk, D. W., Witkowski, A., Moros, M., Lloyd, J. M., Høyer, J. L., Miettinen, A., & Kuijpers, A. (2017). Quantitative reconstruction of Holocene sea ice and sea surface temperature off West Greenland from the first regional diatom data set. *Paleoceanography*, *32*(1), 18–40. https://doi.org/10.1002/2016PA003003

Kremer, A., Stein, R., Fahl, K., Ji, Z., Yang, Z., Wiers, S., et al. (2018). Changes in sea ice cover and ice sheet extent at the Yermak Plateau during the last 160 ka – Reconstructions from biomarker records. *Quaternary Science Reviews*, *182*, 93–108. https://doi.org/10.1016/j.quascirev.2017.12.016

Lajeunesse, P., & St-Onge, G. (2008). The subglacial origin of the Lake Agassiz-Ojibway final outburst flood. *Nature Geoscience*, *1*(3), 184–188. https://doi.org/10.1038/ngeo130

Lamb, H. F. (1984). Modern pollen spectra from Labrador and their use in reconstructing Holocene vegetational history. *Journal of Ecology*, *72*(1), 37–59. https://doi.org/10.2307/2260005

Laskar, J., Robutel, P., Joutel, F., Gastineau, M., Correia, A. C. M., & Levrard, B. (2004). A longterm numerical solution for the insolation quantities of the Earth. *Astronomy & Astrophysics*, *428*(1), 261–285. https://doi.org/10.1051/0004-6361:20041335

Lazier, J. R. N., & Wright, D. G. (1993). Annual velocity variations in the Labrador Current. *Journal of Physical Oceanography*, *23*(4), 659–678. https://doi.org/10.1175/1520-0485(1993)023<0659:AVVITL>2.0.CO;2

LeGrande, A. N., & Schmidt, G. A. (2008). Ensemble, water isotope-enabled, coupled general circulation modeling insights into the 8.2 ka event. *Paleoceanography*, *23*(3), PA3207. https://doi.org/10.1029/2008PA001610

Levac, E. (2001). High resolution Holocene palynological record from the Scotian Shelf. *Marine Micropaleontology*, *43*(3–4), 179–197. https://doi.org/10.1016/s0377-8398(01)00033-0

Lewis, C. F. M., Miller, A. A. L., Levac, E., Piper, D. J. W., & Sonnichsen, G. V. (2012). Lake Agassiz outburst age and routing by Labrador Current and the 8.2 cal ka cold event. *Quaternary International*, *260*, 83–97. https://doi.org/10.1016/j.quaint.2011.08.023

Limoges, A., Ribeiro, S., Weckström, K., Heikkilä, M., Zamelczyk, K., Andersen, T. J., et al. (2018). Linking the modern distribution of biogenic proxies in high Arctic Greenland shelf sediments to sea ice, primary production, and Arctic-Atlantic inflow. *Journal of Geophysical Research: Biogeosciences*, *123*(3), 760–786. https://doi.org/10.1002/2017JG003840

Limoges, A., Weckström, K., Ribeiro, S., Georgiadis, E., Hansen, K. E., Martinez, P., et al. (2020). Learning from the past: Impact of the Arctic Oscillation on sea ice and marine productivity off northwest Greenland over the last 9,000 years. *Global Change Biology*, *26*(12), 6767–6786. https://doi.org/10.1111/gcb.15334

Lochte, A. A., Repschläger, J., Kienast, M., Garbe-Schönberg, D., Andersen, N., Hamann, C., & Schneider, R. (2019a). Labrador Sea freshening at 8.5 ka BP caused by Hudson Bay Ice Saddle collapse. *Nature Communications*, *10*(1), 1–9. https://doi.org/10.1038/s41467-019-08408-6

Lochte, A. A., Repschläger, J., Seidenkrantz, M. S., Kienast, M., Blanz, T., & Schneider, R. R. (2019b). Holocene water mass changes in the Labrador Current. *Holocene*, *29*(4), 676–690. https://doi.org/10.1177/0959683618824752

Lochte, A. A., Schneider, R., Kienast, M., Repschläger, J., Blanz, T., Garbe-Schönberg, D., & Andersen, N. (2020). Surface and subsurface Labrador Shelf water mass conditions during the last 6000 years. *Climate of the Past*, *16*(4), 1127–1143. https://doi.org/10.5194/cp-16-1127-2020

MacLean, B. (2001). Introduction: Geographic setting and studies. *Bulletin of the Geological Survey of Canada*, *566*, 5–17.

Mathis, M., & Mikolajewicz, U. (2020). The impact of meltwater discharge from the Greenland ice sheet on the Atlantic nutrient supply to the northwest European shelf. *Ocean Science*, *16*(1), 167–193. https://doi.org/10.5194/os-16-167-2020

McNeely, R., Dyke, A. S., & Southon, J. R. (2006). Canadian marine reservoir ages, preliminary data assessment. https://doi.org/10.4095/221564

Meissner, K. J., & Clark, P. U. (2006). Impact of floods versus routing events on the thermohaline circulation. *Geophysical Research Letters*, *33*(15), L15704. https://doi.org/10.1029/2006GL026705

Mortlock, R. A., & Froelich, P. N. (1989). A simple method for the rapid-determination of biogenic opal in Pelagic marine-sediments. *Deep Sea Research Part A. Oceanographic Research Papers*, *36*(9), 1415–1426. https://doi.org/10.1016/0198-0149(89)90092-7

Müller, J., Wagner, A., Fahl, K., Stein, R., Prange, M., & Lohmann, G. (2011). Towards quantitative sea ice reconstructions in the northern North Atlantic: A combined biomarker and numerical modelling approach. *Earth and Planetary Science Letters*, *306*(3–4), 137–148. https://doi.org/10.1016/j.epsl.2011.04.011

Müller, J., Werner, K., Stein, R., Fahl, K., Moros, M., & Jansen, E. (2012). Holocene cooling culminates in sea ice oscillations in Fram Strait. *Quaternary Science Reviews*, *47*, 1–14. https://doi.org/10.1016/j.quascirev.2012.04.024

Muschitiello, F., D'Andrea, W. J., Schmittner, A., Heaton, T. J., Balascio, N. L., DeRoberts, N., et al. (2019). Deep-water circulation changes lead North Atlantic climate during deglaciation. *Nature Communications*, *10*(1), 1272. https://doi.org/10.1038/s41467-019-09237-3

Myers, P. G., Donnelly, C., & Ribergaard, M. H. (2009). Structure and variability of the West Greenland Current in Summer derived from 6 repeat standard sections. *Progress in Oceanography*, *80*(1–2), 93–112. https://doi.org/10.1016/j.pocean.2008.12.003

Nelson, D. M., Treguer, P., Brzezinski, M. A., Leynaert, A., & Queguiner, B. (1999). Production and dissolution of biogenic silica in the ocean: Revised global estimates, comparison with regional data and relationship to biogenic sedimentation. *Global Biogeochemical Cycles*, *9*(3), 359–372. https://doi.org/10.1029/95gb01070

Olsen, J., Anderson, N. J., & Knudsen, M. F. (2012). Variability of the North Atlantic Oscillation over the past 5,200 years. *Nature Geoscience*, *5*(11), 1–14. https://doi.org/10.1038/ngeo1589

Oster, J. L., Sharp, W. D., Covey, A. K., Gibson, J., Rogers, B., & Mix, H. (2017). Climate response to the 8.2 ka event in coastal California. *Scientific Reports*, *7*(1), 3886. https://doi.org/10.1038/s41598-017-04215-5

Park, J., Park, J., Yi, S., Cheul Kim, J., Lee, E., & Choi, J. (2019). Abrupt Holocene climate shifts in coastal East Asia, including the 8.2 ka, 4.2 ka, and 2.8 ka BP events, and societal responses on the Korean peninsula. *Scientific Reports*, *9*(1), 10806. https://doi.org/10.1038/s41598-019-47264-8

Petrie, B. (2007). Does the North Atlantic Oscillation affect hydrographic properties on the Canadian Atlantic Continental Shelf? *Atmosphere - Ocean*, *45*(3), 141–151. https://doi.org/10.3137/ao.450302

Petrie, B., & Anderson, C. (1983). Circulation on the newfoundland continental shelf. *Atmosphere - Ocean*, *21*(2), 207–226. https://doi.org/10.1080/07055900.1983.9649165

Pickart, R. S., Torres, D. J., & Clarke, R. A. (2002). Hydrography of the Labrador Sea during active convection. *Journal of Physical Oceanography*, *32*(2), 428–457. https://doi.org/10.1175/1520-0485(2002)032<0428:HOTLSD>2.0.CO;2

Prinsenberg, S. J., Peterson, I. K., Narayanan, S., & Umoh, J. U. (1997). Interaction between atmosphere, ice cover, and ocean off Labrador and Newfoundland from 1962 to 1992. *Canadian Journal of Fisheries and Aquatic Sciences*, *54*(S1), 30–39. https://doi.org/10.1139/f96-150

Ragueneau, O., Tréguer, P., Leynaert, A., Anderson, R. F., Brzezinski, M. A., DeMaster, D. J., et al. (2000). A review of the Si cycle in the modern ocean: Recent progress and missing gaps in the application of biogenic opal as a paleoproductivity proxy. *Global and Planetary Change*, *26*(4), 317–365. https://doi.org/10.1016/S0921-8181(00)00052-7

Rahmstorf, S. (1994). Rapid climate transitions in a coupled ocean–atmosphere model. *Nature*, *372*(6501), 82–85. https://doi.org/10.1038/372082a0

Ramsey, C. B. (2008). Deposition models for chronological records. *Quaternary Science Reviews*, *27*(1–2), 42–60. https://doi.org/10.1016/j.quascirev.2007.01.019

Ramsey, C. B. (2009). Bayesian analysis of radiocarbon dates. *Radiocarbon*, *51*(1), 337–360. https://doi.org/10.1017/S0033822200033865

Rashid, H., Piper, D. J., Drapeau, J., Marin, C., & Smith, M. E. (2019). Sedimentology and history of sediment sources to the NW Labrador Sea during the past glacial cycle. *Quaternary Science Reviews*, *221*, 105880. https://doi.org/10.1016/j.quascirev.2019.105880

Rashid, H., Piper, D. J., Lazar, K. B., McDonald, K., & Saint-Ange, F. (2017). The Holocene Labrador Current: Changing linkages to atmospheric and oceanographic forcing factors. *Paleoceanography*, *32*(5), 498–510. https://doi.org/10.1002/2016pa003051

Rashid, H., Piper, D. J. W., Mansfield, C., Saint-Ange, F., & Polyak, L. (2014). Signature of the Gold Cove event (10.2ka) in the Labrador Sea. *Quaternary International*, *352*(C), 212–221. https://doi.org/10.1016/j.quaint.2014.06.063

Rasmussen, S. O., Andersen, K. K., Svensson, A. M., Steffensen, J. P., Vinther, B. M., Clausen, H. B., et al. (2006). A new Greenland ice core chronology for the last glacial termination. *Journal of Geophysical Research*, *111*(6), D06102. https://doi.org/10.1029/2005JD006079

Rasmussen, S. O., Vinther, B. M., Clausen, H. B., & Andersen, K. K. (2007). Early Holocene climate oscillations recorded in three Greenland ice cores. *Quaternary Science Reviews*, *26*(15–16), 1907–1914. https://doi.org/10.1016/j.quascirev.2007.06.015

Ribeiro, S., Sejr, M. K., Limoges, A., Heikkilä, M., Andersen, T. J., Tallberg, P., et al. (2017). Sea ice and primary production proxies in surface sediments from a High Arctic Greenland fjord: Spatial distribution and implications for palaeoenvironmental studies. *Ambio*, *46*(S1), 106–118. https://doi.org/10.1007/s13280-016-0894-2

Richerol, T., Fréchette, B., Rochon, A., & Pienitz, R. (2016). Holocene climate history of the Nunatsiavut (northern Labrador, Canada) established from pollen and dinoflagellate cyst assemblages covering the past 7000 years. *The Holocene*, *26*(1), 44–60. https://doi.org/10.1177/095968361559682

Rohling, E. J., & Pälike, H. (2005). Centennial-scale climate cooling with a sudden cold event around 8,200 years ago. *Nature*, *434*(7036), 975–979. https://doi.org/10.1038/nature03421

Rontani, J. F., Charrière, B., Sempéré, R., Doxaran, D., Vaultier, F., Vonk, J. E., & Volkman, J. K. (2014). Degradation of sterols and terrigenous organic matter in waters of the Mackenzie Shelf, Canadian Arctic. *Organic Geochemistry*, *75*, 61–73. https://doi.org/10.1016/j.orggeochem.2014.06.002

Rowland, S. J., Allard, W. G., Belt, S. T., Massé, G., Robert, J. M., Blackburn, S., et al. (2001). Factors influencing the distributions of polyunsaturated terpenoids in the diatom, Rhizosolenia setigera. *Phytochemistry*, *58*(5), 717–728. https://doi.org/10.1016/S0031-9422(01)00318-1

Saini, J., Stein, R., Fahl, K., Weiser, J., Hebbeln, D., Hillaire-Marcel, C., & de Vernal, A. (2020). Holocene variability in sea ice and primary productivity in the Northeastern Baffin Bay. *Arktos*, *6*(1–3), 55–73. https://doi.org/10.1007/s41063-020-00075-y

Saini, J., Stein, R., Fahl, K., Weiser, J., Hebbeln, D., & Madaj, L. (2022). Holocene variability in sea-ice conditions in the eastern Baffin Bay-Labrador Sea – A north–south biomarker transect study. *Boreas*, *51*(3), 553–572. https://doi.org/10.1111/bor.12583

Sakshaug, E. (2004). Primary and secondary production in the Arctic Seas. In R. Stein & R. W. Macdonald (Eds.), *The organic carbon cycle in the Arctic Ocean* (pp. 57–81). https://doi.org/10.1007/978-3-642-18912-8

Schneider, R. R., Blanz, T., Evers, F., Gasparatto, F., Gross, F., Hüls, M., et al. (2016). Maria S. Merian Berichte, Paleoclimate Understanding Labrador Sea (PULSE) Cruise No. MSM45.

Seidenkrantz, M. S. (2013). Benthic foraminifera as palaeo sea-ice indicators in the subarctic realm - Examples from the Labrador Sea-Baffin Bay region. *Quaternary Science Reviews*, *79*, 135–144. https://doi.org/10.1016/j.quascirev.2013.03.014

Sheldon, C. M., Seidenkrantz, M. S., Pearce, C., Kuijpers, A., Hansen, M. J., & Christensen, E. Z. (2016). Holocene oceanographic changes in SW Labrador Sea, off Newfoundland. *The Holocene*, *26*(2), 274–289. https://doi.org/10.1177/09596836156086

Smik, L., & Belt, S. T. (2017). Distributions of the Arctic sea ice biomarker proxy IP25 and two phytoplanktonic biomarkers in surface sediments from West Svalbard. *Organic Geochemistry*, *105*, 39–41. https://doi.org/10.1016/j.orggeochem.2017.01.005

Smik, L., Cabedo-Sanz, P., & Belt, S. T. (2016). Semi-quantitative estimates of paleo Arctic sea ice concentration based on source-specific highly branched isoprenoid alkenes: A further development of the PIP25 index. *Organic Geochemistry*, *92*, 63–69. https://doi.org/10.1016/j.orggeochem.2015.12.007

Solignac, S., De Vernal, A., & Hillaire-Marcel, C. (2004). Holocene sea-surface conditions in the North Atlantic - Contrasted trends and regimes in the western and eastern sectors (Labrador Sea vs. Iceland Basin). *Quaternary Science Reviews*, *23*(3–4), 319–334. https://doi.org/10.1016/j.quascirev.2003.06.003

Solignac, S., Seidenkrantz, M. S., Jessen, C., Kuijpers, A., Gunvald, A. K., & Olsen, J. (2011). Late-Holocene sea-surface conditions offshore Newfoundland based on dinoflagellate cysts. *The Holocene*, *21*(4), 539–552. https://doi.org/10.1177/09596836103857

Stein, R., & Fahl, K. (2013). Biomarker proxy shows potential for studying the entire Quaternary Arctic sea ice history. *Organic Geochemistry*, *55*, 98–102. https://doi.org/10.1016/j.orggeochem.2012.11.005

Stein, R., Fahl, K., Gierz, P., Niessen, F., & Lohmann, G. (2017a). Arctic Ocean sea ice cover during the penultimate glacial and the last interglacial. *Nature Communications*, *8*(1), 373. https://doi.org/10.1038/s41467-017-00552-1

Stein, R., Fahl, K., Schade, I., Manerung, A., Wassmuth, S., Niessen, F., & Nam, S. I. (2017b). Holocene variability in sea ice cover, primary production, and Pacific-Water inflow and climate change in the Chukchi and East Siberian Seas (Arctic Ocean). *Journal of Quaternary Science*, *32*(3), 362–379. https://doi.org/10.1002/jqs.2929

Stein, R., Fahl, K., Schreck, M., Knorr, G., Niessen, F., Forwick, M., et al. (2016). Evidence for ice-free summers in the late Miocene central Arctic Ocean. *Nature Communications*, *7*(1), 11148. https://doi.org/10.1038/ncomms11148

Stein, R., & Macdonal, R. W. (2004). *The organic carbon cycle in the Arctic Ocean*. Springer.

Stocker, T. F., & Wright, D. G. (1991). Rapid transitions of the ocean's deep circulation induced by changes in surface water fluxes. *Nature*, *351*(6329), 729–732. https://doi.org/10.1038/351729a0

Stocker, T. F., Wright, D. G., & Broecker, W. S. (1992). The influence of high-latitude surface forcing on the global thermohaline circulation. *Paleoceanography*, *7*(5), 529–541. https://doi.org/10.1029/92PA01695

Sundal, A. V., Shepherd, A., Nienow, P., Hanna, E., Palmer, S., & Huybrechts, P. (2011). Melt-induced speed-up of Greenland ice sheet offset by efficient subglacial drainage. *Nature*, *469*(7331), 521–524. https://doi.org/10.1038/nature09740

Thomas, E. R., Wolff, E. W., Mulvaney, R., Steffensen, J. P., Johnsen, S. J., Arrowsmith, C., et al. (2007). The 8.2 ka event from Greenland ice cores. *Quaternary Science Reviews*, *26*(1–2), 70–81. https://doi.org/10.1016/j.quascirev.2006.07.017

Trouet, V., Esper, J., Graham, N. E., Baker, A., Scourse, J. D., & Frank, D. C. (2009). Persistent positive North Atlantic Oscillation mode dominated the medieval climate anomaly. *Science*, *324*(5923), 78–80. https://doi.org/10.1126/science.1166349

Vinther, B. M., Andersen, K. K., Jones, P. D., Briffa, K. R., & Cappelen, J. (2006). Extending Greenland temperature records into the late eighteenth century. *Journal of Geophysical Research*, *111*(11), 1–13. https://doi.org/10.1029/2005JD006810

Volkman, J. K. (1986). A review of sterol markers for marine and terrigenous organic matter. *Organic Geochemistry*, *9*(2), 83–99. https://doi.org/10.1016/0146-6380(86)90089-6

Volkman, J. K., Revill, A. T., Holdsworth, D. G., & Fredericks, D. (2008). Organic matter sources in an enclosed coastal inlet assessed using lipid biomarkers and stable isotopes. *Organic Geochemistry*, *39*(6), 689–710. https://doi.org/10.1016/j.orggeochem.2008.02.014

von Appen, W. J., Waite, A. M., Bergmann, M., Bienhold, C., Boebel, O., Bracher, A., et al. (2021). Sea-ice derived meltwater stratification slows the biological carbon pump: Results from continuous observations. *Nature Communications*, *12*(1), 1–16. https://doi.org/10.1038/s41467-021-26943-z

Weiser, J., Titschack, J., Kienast, M., McCave, I. N., Lochte, A. A., Saini, J., et al. (2021). Atlantic water inflow to Labrador Sea and its interaction with ice sheet dynamics during the Holocene. *Quaternary Science Reviews*, *256*, 106833. https://doi.org/10.1016/j.quascirev.2021.106833

Wiersma, A. P., & Jongma, J. I. (2010). A role for icebergs in the 8.2 ka climate event. *Climate Dynamics*, *35*(2), 535–549. https://doi.org/10.1007/s00382-009-0645-1

Wiersma, A. P., & Renssen, H. (2006). Model-data comparison for the 8.2 ka BP event: Confirmation of a forcing mechanism by catastrophic drainage of Laurentide Lakes. *Quaternary Science Reviews*, *25*(1–2), 63–88. https://doi.org/10.1016/j.quascirev.2005.07.009

Wiersma, A. P., Renssen, H., Goosse, H., & Fichefet, T. (2006). Evaluation of different freshwater forcing scenarios for the 8.2 ka BP event in a coupled climate model. *Climate Dynamics*, *27*(7–8), 831–849. https://doi.org/10.1007/s00382-006-0166-0

Williams, J. J., Gourmelen, N., Nienow, P., Bunce, C., & Slater, D. (2021). Helheim glacier poised for dramatic retreat. *Geophysical Research Letters*, *48*(23), e2021GL094546. https://doi.org/10.1029/2021GL094546

Xiao, X., Fahl, K., & Stein, R. (2013). Biomarker distributions in surface sediments from the Kara and Laptev seas (Arctic Ocean): Indicators for organic-carbon sources and sea-ice coverage. *Quaternary Science Reviews*, *79*, 40–52. https://doi.org/10.1016/j.quascirev.2012.11.028

Xiao, X., Stein, R., & Fahl, K. (2015). MIS 3 to MIS 1 temporal and LGM spatial variability in Arctic Ocean sea ice cover: Reconstruction from biomarkers. *Paleoceanography*, *30*(7), 969–983. https://doi.org/10.1002/2015PA002814

Yang, Y., & Piper, D. J. W. (2021). Alongflow variability of the Labrador Current during the Holocene. *Quaternary Science Reviews*, *267*, 107110. https://doi.org/10.1016/j.quascirev.2021.107110

You, D., Stein, R., Fahl, K., Williams, M. C., Schmidt, D. N., Mc Cave, I. N., et al. (2023). Last deglacial abrupt climate changes caused by meltwater pulses in the Labrador Sea. *Communications Earth & Environment*, *4*(1), 81. https://doi.org/10.1038/s43247-023-00743-3

Yu, S. Y., Colman, S. M., Lowell, T. V., Milne, G. A., Fisher, T. G., Breckenridge, A., et al. (2010). Freshwater outburst from lake superior as a trigger for the cold event 9300 years ago. *Science*, *328*(5983), 1262–1266. https://doi.org/10.1126/science.1187860

Yunker, M. B., Macdonald, R. W., Veltkamp, D. J., & Cretney, W. J. (1995). Terrestrial and marine biomarkers in a seasonally ice-covered Arctic estuary - Integration of multivariate and biomarker approaches. *Marine Chemistry*, *49*(1), 1–50. https://doi.org/10.1016/0304-4203(94)00057-K